Chapter

6

Daylight Coefficients: Formulation, Validation and Application

"Funding for this work... would be nice."

GREG WARD (RE: MGF)

This chapter describes how time varying daylight illumination can be both accurately and efficiently predicted for arbitrary sky and sun conditions. The prediction technique is based on the daylight coefficient approach. The accuracy of the daylight coefficient derived illuminance predictions is verified using the BRE-IDMP validation dataset. The chapter concludes with a series of examples that demonstrate how daylight coefficients can be used to predict the daylight illumination for an entire year on an hourly basis.

6.1 Introduction

The seasonal and daily variations in daylight follow a typical pattern, Figure 6-1. These two contour plots show calculated means of global and diffuse horizontal illuminance based on ten years of measurements taken

at Kew, UK [Hunt 79]. The dashed lines indicate the start and finish of the normal working day; 09:00 to 17:30 hrs. LAT is the local apparent time which approximates to GMT for this location. The cumulative diffuse illuminance availability can be shown as the percentage of the working year for which a given diffuse illuminance is exceeded, Figure 6-2.

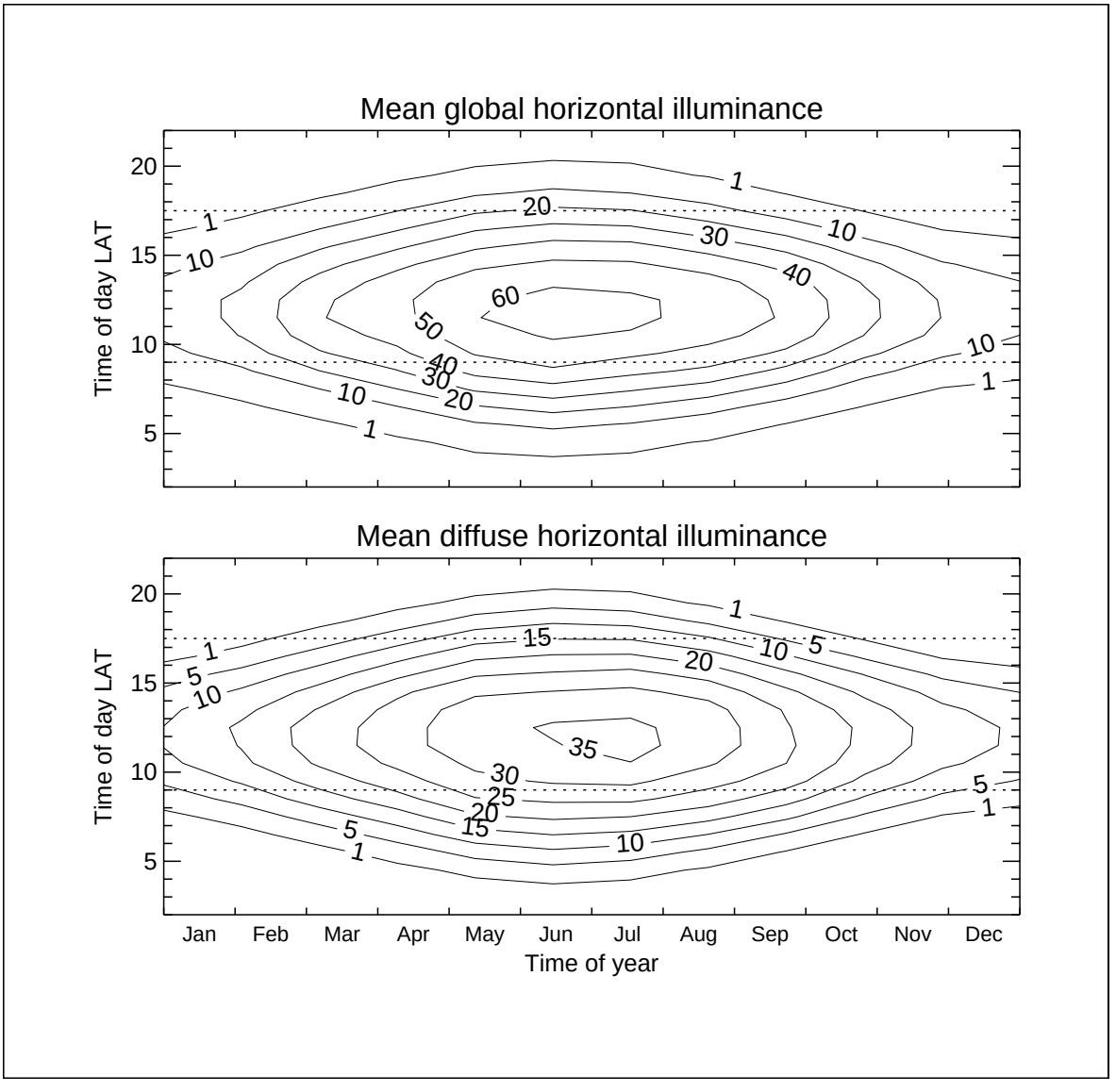

Figure 6-1. Global and diffuse illuminance availability (klux)

6.1.1 The daylight factor approach to annual estimates

The daylight factor approach is invariably used to assess the potential of a design to provide useful levels of daylight illumination. The approach - described in Section 2.2.1 - uses the CIE standard overcast sky, irrespective of the prevailing climatic conditions for the locale of the proposed design. And of course, the contribution of sunlight to internal illuminance is not modelled using this approach. Applying a simple technique, cumulative internal illuminance availability can be calculated from daylight factor values and charts of cumulative diffuse sky illuminance. This gives a first order approximation to annual daylighting provision from which supplementary lighting requirements can be estimated.

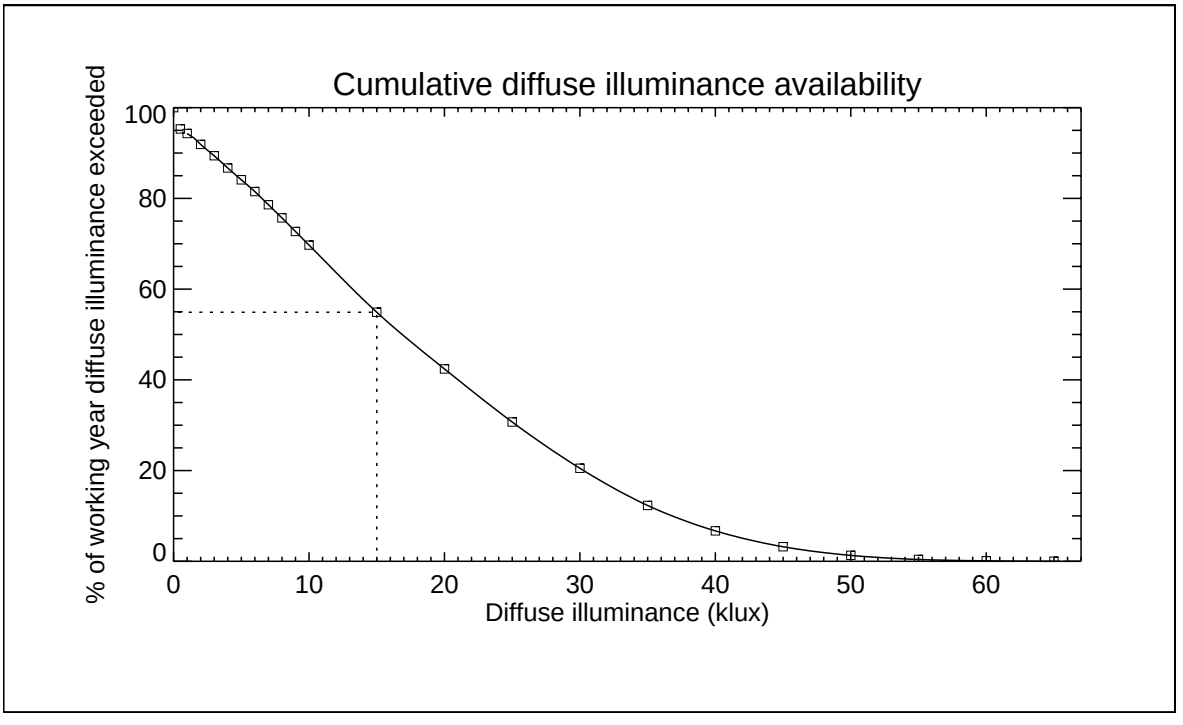

Figure 6-2. Cumulative diffuse illuminance

Example

Suppose that the minimum required internal illuminance at a point in an office is 500 lux, and that a daylight factor evaluation using the CIE standard overcast sky (equation, scale-model or simulation) predicts a

daylight factor value of 3.3%. The minimum diffuse sky illuminance which provides an average internal illuminance of 500 lux, is therefore

$$\frac{500 \times 100}{3.3} = 15{,}000 \text{ lux}$$

It can be determined from Figure 6-2 that a diffuse sky illuminance of 15 klux is exceeded for about 55% of the normal working time.

The CIE standard overcast sky is likely to be a reasonable approximation to some of the duller skies in the cumulative distribution. However, it was demonstrated in the previous chapter that internal illuminance predictions are very sensitive to the sky model type (Section 5.3). Furthermore, only about 40% of the skies in the Kew TRY can be classed as heavily overcast (Figure 3-9). To predict annual daylighting provision with any certainty therefore, predictions need to be based on the full range of naturally occurring sky conditions. Furthermore, the sky models that are used need to be reasonable representations of the naturally occurring sky luminance distributions.[1]

As noted above, the daylight factor method does not account for direct sunlight. It is therefore highly inappropriate for building designs where the redistribution of direct beam radiation to provide diffuse illuminance is a significant feature of the daylighting system. As is the case with designs that make use of light shelves or mirrored louvres.

6.1.2 Annual daylight provision based on varying sky conditions

Luminance distributions that do not conform to the CIE overcast standard have generally been used for specialist studies designed to address specific issues, e.g. solar penetration or shading for particular times of the day or year. Typically, only a few cases are modelled and the results have little

1. Or even an annual time-series of measured sky luminance distributions. But since several years data are needed to synthesise a ‘statistically average’ year, it is unlikely that such a dataset will emerge for some time.

relevance to the long term daylighting potential of a space. A true measure of the long-term daylighting potential for a building must account for the internal illuminances produced by *all* the skies measured at or near the intended site over a monitoring period of, ideally, a full year or more. Such an evaluation would typically adopt the following procedure [Littlefair 92]:

- Obtain basic climate data from a weather tape, usually global and diffuse irradiance.
- Convert the irradiance data to external horizontal illuminances using a luminous efficacy model.
- Generate a sky luminance distribution using a sky model.
- Use the sky luminance distribution to calculate internal illuminances.
- Determine the artificial lighting requirements using a lighting control algorithm.
- Calculate the resultant heat gains produced by the lighting (if the lighting simulation is to be part of an integrated buildings energy analysis program).

If measurements were obtained as hourly integrated values, as is generally the case with weather tapes, a normal working year would contain data for approximately 3,500 skies. With the latest generation multi-processor workstations, modelling several thousand individual cases is a tractable, though still rather time consuming, task. A more efficient solution method might be the daylight coefficient approach [Tregenza 83]. This technique eliminates the need to perform the most computationally demanding part of the simulation - the inter-reflection calculation - for every individual case, i.e. ~3,500 skies for a full year. The daylight coefficient approach requires that the sky be broken into many patches. The internal illuminance at a point that results from a patch of unit-luminance sky is computed and cached. This is done for each patch of sky. It is then possible, in principle, to determine the internal illuminance for an arbitrary sky luminance

distribution (and sun luminance/position) using relatively simple (i.e. quick) arithmetic operations on matrices. The computational expense of a daylight coefficient calculation for a sky with *N* patches is comparable to that for *N* standard calculations. Provided therefore that the number of patches is less than the number of skies that need to be modelled, the technique has the potential to be computationally more efficient than treating each sky individually.

6.2 Daylight coefficients: Fundamentals, prediction and analysis

There is more than one way to calculate daylight coefficients using *Radiance*. The first approach, described below, is called the 'Naive Method', or NM. As will be demonstrated, the Naive Method is the most straightforward way to predict DCs with *Radiance*. Preliminary tests however indicated that, with this approach, the derived internal illuminances were likely to contain significant errors. This led to the formulation of a second approach called the 'Refined Method' (RM), which was designed to overcome the imprecision of the Naive Method. For the RM, two different sky discretisation resolutions and their consequences were examined: they are referred to as the 'Default' and 'Finescale' discretisation schemes. These lead to the possibility of several variants of the final daylight coefficient (DC) formulation for the Refined Method. The two methods (NM and RM) are described below, and the daylight coefficients calculated using both are presented and analysed. There is then a simple comparison test that demonstrates the weakness of the Naive Method.

6.2.1 Fundamentals

If $\Delta E_{\gamma\alpha}$ is the total illuminance produced at a point in a room by a small element of sky at altitude γ and azimuth α, then the daylight coefficient is defined as

$$D_{\gamma\alpha} = \frac{\Delta E_{\gamma\alpha}}{L_{\gamma\alpha}\Delta S_{\gamma\alpha}} \quad \textbf{(6-1)}$$

where $L_{\gamma\alpha}$ is the luminance of the element of sky and $\Delta S_{\gamma\alpha}$ is the solid angle of the patch of sky, Figure 6-3.

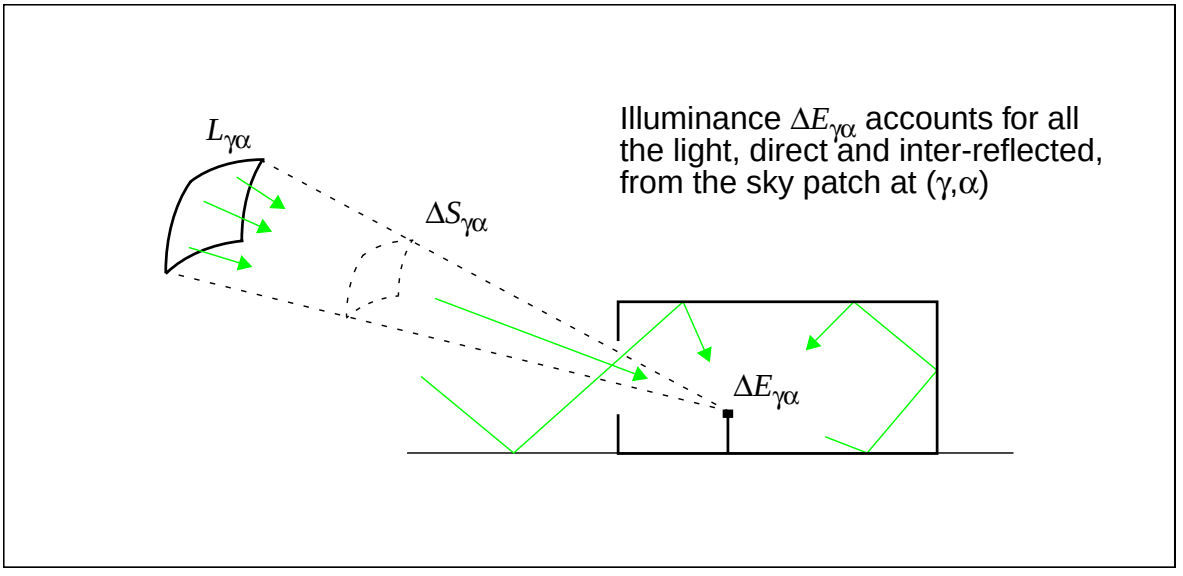

Figure 6-3. Daylight coefficient basics

The magnitude of the daylight coefficient $D_{\gamma\alpha}$ will depend on the physical characteristics of the room and the external environment, e.g. room geometry, surface reflectances, glazing transmissivity, outside obstructions and reflections etc. It is, however, independent of the distribution of luminance across the sky vault, since $\Delta E_{\gamma\alpha}$ varies in proportion to $L_{\gamma\alpha}$. The total illuminance E produced at the point in the room is then calculated from:

$$E = \int_0^{2\pi} \int_0^{\pi/2} D_{\gamma\alpha} L_{\gamma\alpha} \cos\gamma \, d\gamma \, d\alpha \qquad \textbf{(6-2)}$$

It is possible to determine a functional form for daylight coefficients (DCs) for idealised scenes, such as an unobstructed horizontal surface [Tregenza 83]. However, some form of finite element calculation is needed for even the simplest realistic scene.

If the sky were divided into *n* angular zones, then for numerical evaluation, Eq 6-2 can be formulated as:

$$E = \sum_{p=1}^{n} D_p \, S_p \, L_p \qquad \textbf{(6-3)}$$

This gives the illuminance as sum of *n* products of *D*, *S* and *L*, for each patch of sky *p*. The *n* values of *D*, *S* and *L* can therefore be treated as vectors e.g. $\mathbf{D} = \left[D_1, D_2, \ldots, D_n \right]$. The formulation may be expanded to account for *m* points in the room. The array of daylight coefficients then becomes a *m* x *n* matrix. The internal illuminances will then be described by a column vector **E** containing *m* elements. Similarly, another column vector, **c**, can be formed from the *n* products of angular size and luminance. This gives the compact matrix formulation

$$\mathbf{E} = \mathbf{D} \times \mathbf{c} \qquad \textbf{(6-4)}$$

or in expanded form,

$$\begin{bmatrix} E_1 \\ E_2 \\ : \\ E_m \end{bmatrix} = \begin{bmatrix} D_{11} & D_{12} & \ldots & D_{1n} \\ D_{21} & D_{22} & \ldots & D_{2n} \\ : & : & & \\ D_{m1} & D_{m2} & & D_{mn} \end{bmatrix} \times \begin{bmatrix} S_1 \, L_1 \\ S_2 \, L_2 \\ : \quad : \\ : \quad : \\ : \quad : \\ S_n \, L_n \end{bmatrix} \qquad \textbf{(6-5)}$$

This is what may be called the standard daylight coefficient formulation as presented in the original paper [Tregenza 83]. That paper includes a theoretical discussion which describes, in general terms, how individual components of the daylight coefficient matrix (DCM) may be evaluated. The components account separately for the externally reflected light, the direct light and the internally reflected light. A later paper, also theoretical, describes how DCs might be used for the practical computation of internal illuminances [Littlefair, 92]. That paper includes several recommendations

for a practical implementation of the daylight coefficient approach. Some of these were found useful for the work described below, others were not. The final form of the most successful DC implementation described below was dictated in part by *Radiance's* own, unique calculation algorithms.

6.2.2 Overview of the discretisation schemes

At the onset, it was the intention to test the accuracy of the DC derived illuminances using the BRE-IDMP validation dataset. Accordingly, the discretisation schemes employed had to have some correspondence to the sampling pattern of the PRC Krochmann sky scanner. The discretisation schemes made use of different shaped patches and of different resolutions. One of these was based on a sub-division of the sky vault that gave complete sky coverage for the sky hemisphere. Here, each patch was bounded by lower and upper values for altitude and azimuth. These segments of sky, although part of a hemisphere, are referred to for brevity as 'rectangular' patches. The other type of discretisation used solid angles which are referred to as 'circular' patches. The underlying pattern for both patch types was identical to the sampling pattern of the Krochmann sky scanner. That is, 145 patches arranged in the same fashion as the scanner pattern, Figure 6-4.

The 145 patch scheme is referred to as the 'Default' discretisation. The effect of a patch scheme that replaced each of 145 'circular' patches with four individual 'circular' patches was also examined. This scheme used 580 patches and is referred to as the 'Finescale' discretisation. The ordering and numbering scheme for the 'Default' discretisation, complete with the altitude and azimuth for each patch centre, is shown in Figure 6-5. The 145 elements are numbered 1 to 145, and count 'clockwise' from North i.e. N $\rightarrow$ E $\rightarrow$ S $\rightarrow$ W. The orientation of the BRE office description relative to the discretised sky is shown at the base of Figure 6-5.

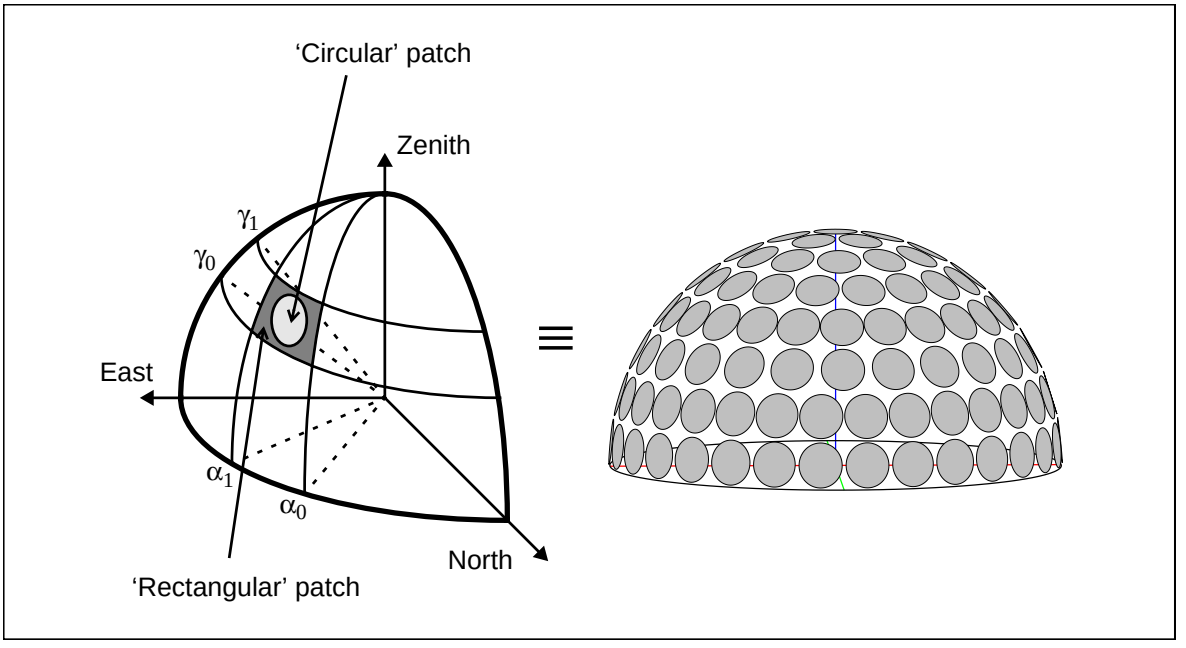

Figure 6-4. DC patch schemes based on scanner measurement pattern

6.2.3 The 'Naive Method'

The 'Naive Method' was based closely on the standard formulation given in Section 6.2.1. For the prediction of the DCs, each luminous sky patch was modelled using a source angle type **`light`**. These are the 'circular' patches described in the previous section. These patches do not, of course, offer complete sky coverage. Note that it is not possible to specify a 'rectangular' source angle in *Radiance* in a straightforward way (this is discussed in later sections). The source angle type **`light`** is sampled with a single ray, which, in the usual mode of use, is directed to the source centre, Figure 6-6.

Thus, the direct component (from the photocell to the source) was calculated using a single ray directed to the source centre.[2] For the indirect component, many sampling rays were used. But here also, for every final light transfer from a surface to the source, a single ray was directed to the

2. Recall that *Radiance* uses backwards ray tracing.

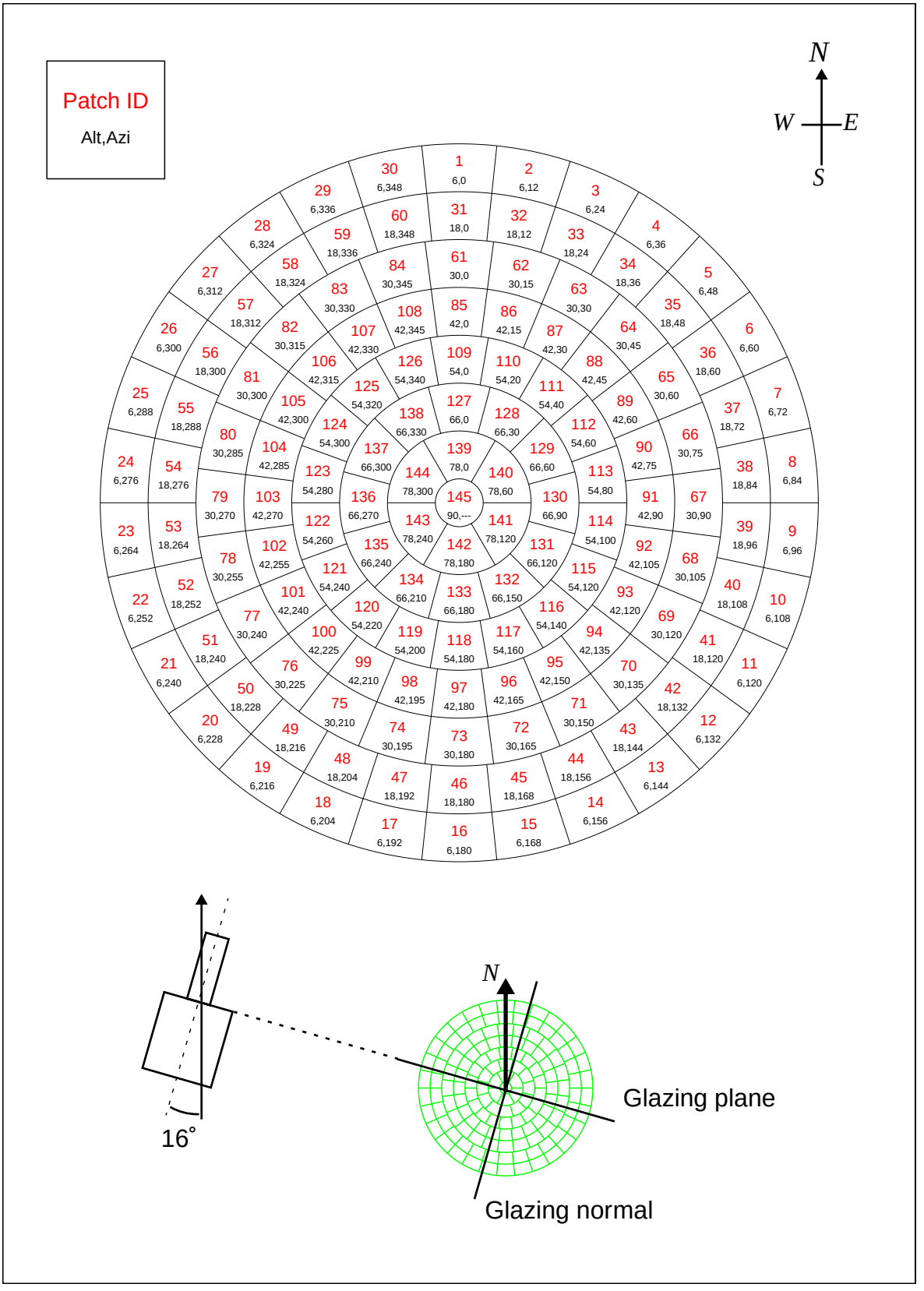

Figure 6-5. Patch ID and building orientation

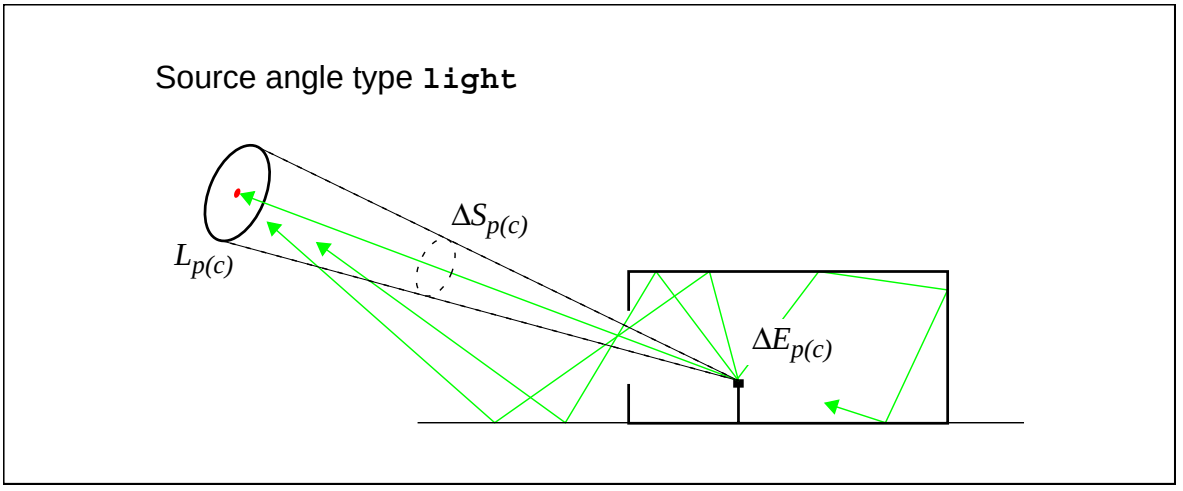

Figure 6-6. The naive formulation

source centre. So, the daylight coefficient for each *patch* was calculated using rays that sampled only the *point* at the patch centre.

The daylight coefficient for the 'circular' patch *p* therefore is:

$$D_p = \frac{\Delta E_{p(c)}}{L_{p(c)} \Delta S_{p(c)}} \quad \textbf{(6-6)}$$

The subscript in parentheses denotes the patch shape, e.g. *(c)* for 'circular' and *(r)* for 'rectangular'. Using this method, the total internal illuminance E_{tot} due to a sky and sun of arbitrary luminance is calculated as the sum of the sky (E_{sky}) and sun (E_{sun}) illuminance components:

$$E_{sky} = \sum_{p=1}^{n} D_p \, \Delta S_{p(r)} \, L_{p(r)}^{sky} \quad \textbf{(6-7)}$$

Note that 'rectangular' patches are now used because the sum of the individual patch solid angles must be equal to the solid angle for a hemisphere:

$$2\pi = \sum_{p=1}^{n} \Delta S_{p(r)} \quad \textbf{(6-8)}$$

In other words - for each patch in turn - the illumination effect of a 'rectangular' patch of sky of uniform luminance is derived using the DC value predicted for one point at the patch centre. The sun component of the illuminance is given by:

$$E_{sun} = D_{\beta} S^{sun} L^{sun} \quad \textbf{(6-9)}$$

where D_{β} is the vector of daylight coefficients for the patch nearest to the sun position, and $S^{sun}L^{sun}$ is the product of the solid angle and luminance of the sun. The total illuminance therefore is:

$$E_{tot} = E_{sky} + E_{sun} \quad \textbf{(6-10)}$$

DC calculation with Radiance

The patch configuration for the Naive Method was equivalent to a sky with 145 'suns', each of source angle 11˚. The ambient parameter combination used to predict daylight coefficients for the NM was the same as the 'basecase' set used for the validation of the standard calculation (Section 3.3.2). With the NM, a patch of sky is, in effect, identical to a sun description in the standard calculation. Both are described using the source material **`light`**, for which single-ray sampling is employed. The source angle therefore has no effect (Section 3.2.3). It was shown in Section 4.5.2 that, source visibility related errors notwithstanding, the internal illuminance for clear sky days (e.g. 102_92, 129_92, 137_92, etc.) was accurately predicted. For these conditions, the sun was the dominant source of illumination. Thus, there was no reason to suspect that the 'basecase' parameter combination would perform any less well for the prediction of daylight coefficients using the Naive Method.[3]

The DCs were predicted using an automated scheme similar to that described in Section 3.3.4. The 145 individual source description files were generated by an IDL procedure and the sequence of simulations was

3. Note also that for the standard calculation there was a sun and a sky, whereas with each DC patch calculation (NM) there was only a 'sun'.

managed by an 'executive' C-shell script. Using the same ambient parameter combination as the standard calculation, the simulation time for the DC prediction was about the same as that needed for 145 skies. The magnitude and the pattern of the DCs predicted at each photocell is discussed below.

Naive Method DCs: Results and Analysis

The DCs predicted at each photocell are given in Figure 6-7. The magnitude is shown using false colours and the individual patches can be matched to a patch number using the key given in Figure 6-5. The DCs for the total illumination (Direct+Indirect) cover a wide range: from 1.695e-05 to 0.6473. The pattern in total DCs at each photocell can be related somewhat to the building geometry. For p_cell 1, which was nearest the window, the DCs are generally larger than for all the other p_cells. The change in the pattern of the high-value DCs (> 0.2, yellow shading) from p_cell 1 to p_cell 6 suggests a decrease in the number of patches that were directly visible.[4] The patterns however are not quite what one might expect: the decrease in the number of high-value DC patches from p_cell 1 to p_cell 2 seems rather too large. Furthermore, both p_cells 2 and 3 have the *same* number - three - of high value DCs, even though the p_cell further away from the window should 'see' fewer patches. These observations are the result of single-ray light source sampling: the source's contribution to direct illuminance was calculated on the basis of total source visibility, or total source occlusion. As a consequence, depending on the position of the calculation point, the direct sky component could be significantly overestimated, or actually predicted to be zero.

To clarify that this was indeed the case, the DCs were re-calculated for the direct component-only. They are shown alongside the total (i.e. Direct+Indirect) DCs in Figure 6-7. A cross (+) marks a zero value. The range in the direct DCs was much narrower: from 0.0854 to 0.618 (for DCs > 0).

4. Compare this pattern with the photocell 'view' renderings in Figure 4-17 on page 119.

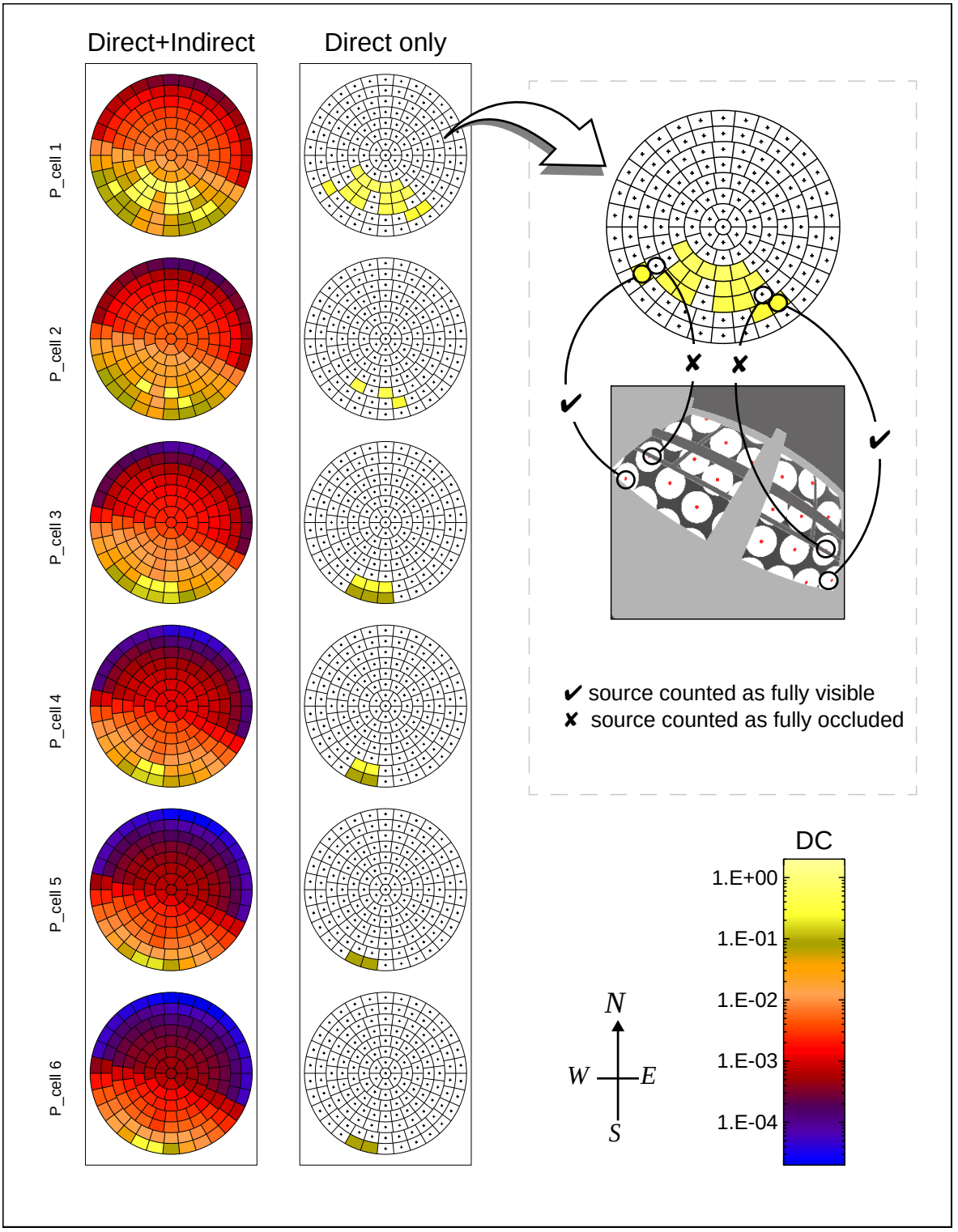

Figure 6-7. Predicted DCs for the NM

Note that the mapping of the magnitude of the predicted DC to colour uses a logarithmic scale

The effects suggested by the total DCs are more readily apparent in the direct-only DCs. In particular, note that there are only three non-zero DCs at p_cell2 and six at p_cell3 (which was further away from the window).

To better understand the effect of single-ray light source sampling, a rendering was created using a special sky description that contained all 145 sky patches. The centre of each 11˚ 'white' source was marked by adding a much smaller 'red' source (1.5˚) to the sky description. The rendering in Figure 6-7 shows a view of this special sky from p_cell 1; the pattern of sky patch visibility/occlusion is related to a (magnified) plot of the predicted DCs. Note how the direct only DC is predicted to be zero when the patch centre is occluded, even though much of the rest of the patch may be visible. It seems likely therefore that, from p_cell 2, the centres of several sky patches were also occluded by glazing frame bars. Note also that, when a source centre was visible from two or more p_cells, the predicted direct DC was the same for all the p_cells. This is because the ray direction to any one patch was identical for all p_cell locations. For all the p_cells that 'see' a particular patch centre, the reduction in the ray luminance due to glazing transmittance (from L to L_g), and therefore the daylight coefficient value, will be identical, Figure 6-8. In contrast, sampling across the source would reveal that it was, say, partially occluded from both positions, though to different degrees (Figure 6-8). Accordingly, direct DCs should have a unique value based on the degree of visibility. This cannot happen when the DC for a *patch* is predicted using a single *point*.

Can *Radiance* be persuaded to sample the source material **`light`** with more than one ray? In principle, yes. Although the method is not straightforward.[5] An alternative approach would be to change the source material to **`glow`** and predict the direct contribution using *Radiance's* indirect calculation, i.e. by hemispherical sampling. With a large number of

5. It involves repeating the direct DC prediction for each patch many times with 'jittering' enabled for the source calculation. With this, rays are randomly distributed over the source. Though with the source material **`light`**, it would still be one ray per source, hence the need for a large number of individual simulations.

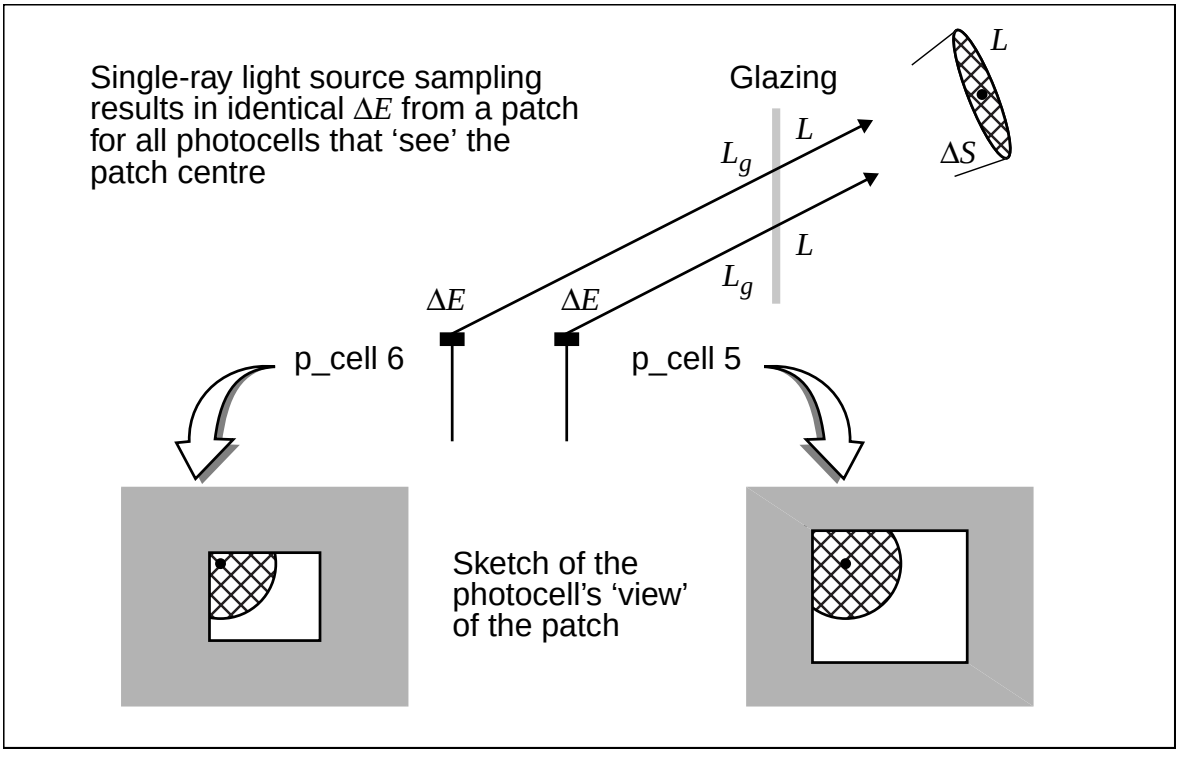

Figure 6-8. Identical DC values for the same patch positions

hemispherical rays, one can be assured that the **glow** source is adequately sampled. This could be demonstrated with convergence tests. However, the technique is very wasteful of sampling rays because an entire hemisphere of rays are spawned to find a relatively small source. And, more importantly, the potential for inaccuracy remains because all the patches taken together do not provide complete sky coverage, Figure 6-9. This rendering shows the 'view' of the sky patches from p_cell 6. Note that the two source centres - counted as visible for the NM direct DCs (p_cell 6 in Figure 6-7) - would both have been counted as fully occluded had the horizontal frame bar been placed a little higher. Both of these issues are addressed in the later sections that describe the 'Refined Method' for calculating DCs.

The Sun Component

Another potential problem with the Naive Method arises when the DCs are used to calculate the illumination from the sun. Significant errors may arise

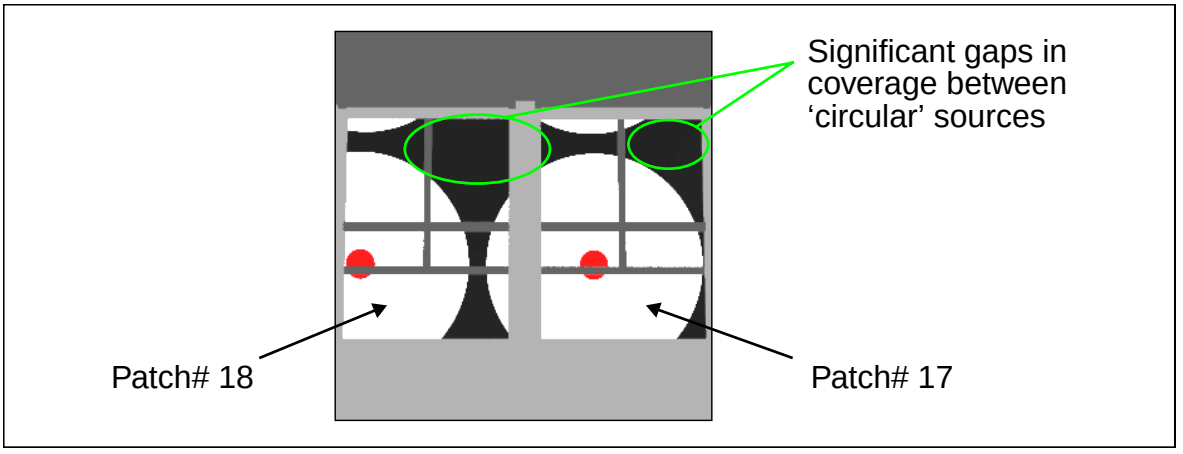

Figure 6-9. Incomplete sky coverage with 'circular' sources

when there is a large difference between the actual sun position and the centre of the nearest patch. This is referred to here as the sun displacement angle (SDA), Figure 6-10. With a patch discretisation based on the scanner

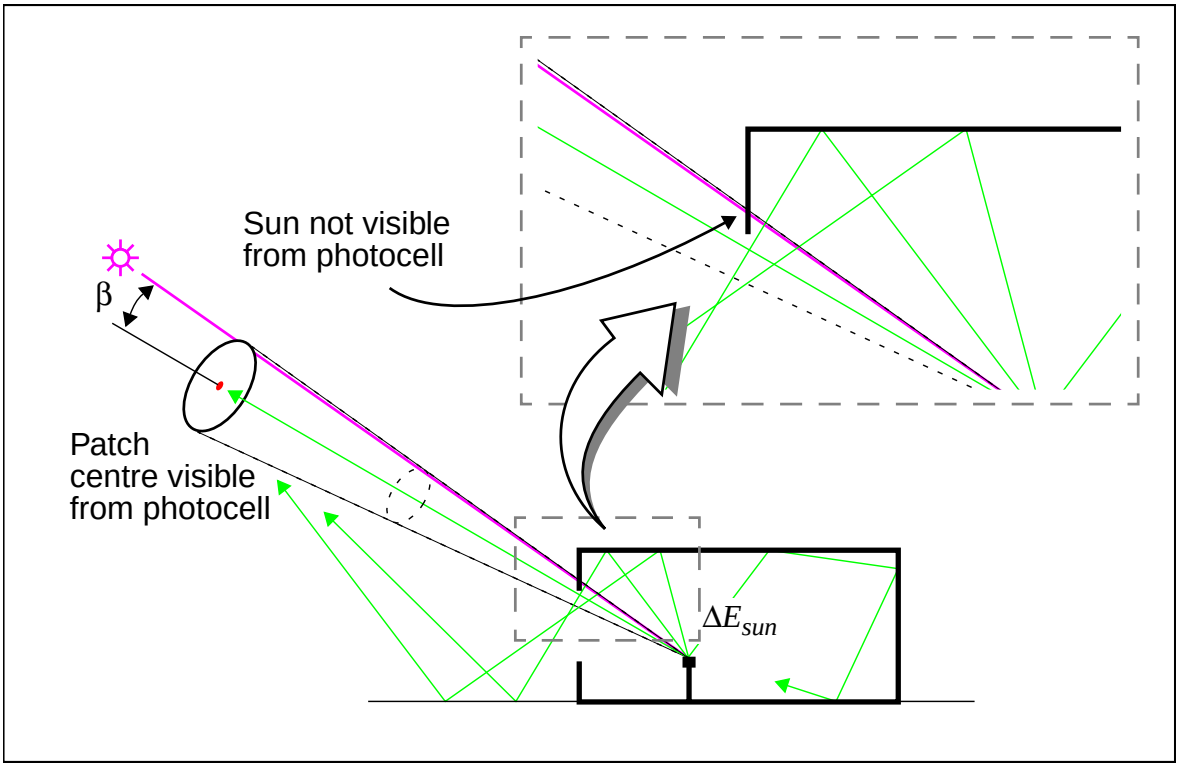

Figure 6-10. Sun displacement angle

pattern (Figure 6-5), the SDA can be as large as 7˚. The greater the SDA, the greater the likelihood that a point is evaluated to be in shade when it was actually illuminated by the sun - or vice-versa. So it is the direct component of illumination from the sun than can be in error the greatest. The indirect component ensues from one or more reflections, and so it is less directional in nature than the direct component. Consequently, the indirect component is generally much less sensitive to the SDA.[6]

Whatever the resolution of the DC patch scheme, there will always be errors in the direct source calculation due to displacement of the sun position. However, these errors could be reduced arbitrarily by using a large number of sources for the *direct sun component only*. For a direct light source calculation, the computational expense is tiny so many thousands of sources could be modelled. The indirect sun component would then be calculated separately using a much smaller number of sources. The separation of the calculation for the direct and indirect sun illuminance components is the first step towards a potentially more accurate and generalised DC scheme. This new scheme, the Refined Method, is described in the following sections.

6.2.4 The 'Default Refined Method'

The potential for imprecision in the direct calculation with the Naive Method could be reduced by increasing the number of individual light sources. In other words, using many points to better approximate the effect of a patch. There is no theoretical limit to the number, or size, of light sources that could be used. However, a simulation would have to be carried out for every source. A more elegant route to achieving the same ends might be to carry out the calculation using 'aimed rays' rather than the irradiance calculation, which has been shown to be prone to light source visibility errors.

6. An exception may be when the sun is just in front of the glazing plane and the SDA is such that the nearest DC patch is just behind, or vice versa.

Aimed Rays

The 'aimed rays' approach requires only one sky vault description, so it eliminates the need to generate hundreds (or thousands) of individual source descriptions. This is possible because source sampling with 'aimed rays' can be precisely controlled by the user. The 'aimed rays' approach is in fact very simple. The **rtrace** program was used to compute the luminance of rays 'aimed' from each photocell location. To do this, **rtrace** was supplied with a list of the ray's origin and direction vectors. The direction vector part of the list is formed from the co-ordinates of an arbitrary number of points evenly distributed over a unit hemisphere. This list was repeated six-fold and 'laminated' to the ray-origin co-ordinates, i.e. the photocell locations. For each ray in the list, **rtrace** computed a luminance value, Figure 6-11.

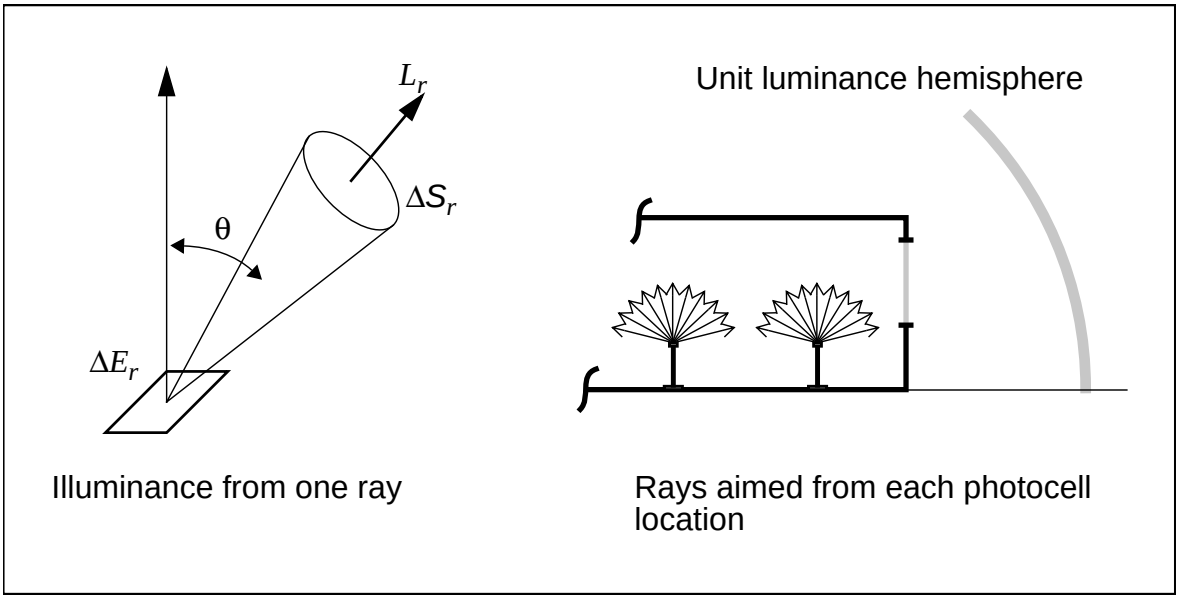

Figure 6-11. 'Aimed' rays

The illuminance at a photocell due to any region of (unit luminance) sky can be determined from the individual ray values for all the rays that intersect with the region of sky. The illuminance due to sky patch *p* is

$$\Delta E_p = \sum_{r \in T} L_r \cos\theta_r \Delta S_r \qquad \textbf{(6-11)}$$

where L_r is the ray luminance, θ_r is the ray zenith angle and ΔS_r is the solid angle associated with the ray. T is the set of rays r that, in an unobstructed scene, intersect with the patch p. The solid angle associated with each ray $\Delta S_r = 2\pi/N_r$, where N_r was the number of rays evenly distributed over the hemisphere.The set T consists of elements r such that, for a rectangular patch of extent $\Delta\alpha$ by $\Delta\gamma$ centred on (α, γ), the set is given by:

$$T = \{r:(\gamma - \Delta\gamma/2) \le \gamma_r < (\gamma + \Delta\gamma/2), (\alpha - \Delta\alpha/2) \le \alpha_r < (\alpha + \Delta\alpha/2)\} \quad \textbf{(6-12)}$$

or for a 'polar-cap' patch:

$$T = \{r:(\pi/2 - \Delta\gamma_z) \le \gamma_r\} \quad \textbf{(6-13)}$$

The DCM for the direct component of illumination was determined using the 'aimed' rays method described above, Figure 6-12(a). A total of 100,366 rays, evenly distributed across the hemisphere, were aimed from each photocell location. Each 'rectangular' patch was sampled by approximately 650 rays (i.e. 100,366/145). The direct DC was computed using Eq 6-1 and Eq 6-11:

$$D_p = \frac{\sum_{r \in T} L_r \cos\theta_r \Delta S_r}{L_p \Delta S_p} = \frac{\sum_{r \in T} L_r \cos\theta_r}{L_p} \quad \textbf{(6-14)}$$

because

$$\sum_{r \in T} \Delta S_r = \Delta S_p \quad \textbf{(6-15)}$$

Note that the individual rays could also be used to construct a direct DCM for all the 100,366 points evenly distributed across the hemisphere e.g.

$$D_r = \frac{L_r \cos\theta_r \Delta S_r}{L_p \Delta S_r} = \frac{L_r \cos\theta_r}{L_p} \quad \textbf{(6-16)}$$

A finely discretised direct DCM could be used in a generalised DC implementation to calculate the direct component of illumination from the sun.[7] A generalised implementation of the DC approach, demonstrated in a later section, includes a discussion on the resolution of the direct sun DCM.

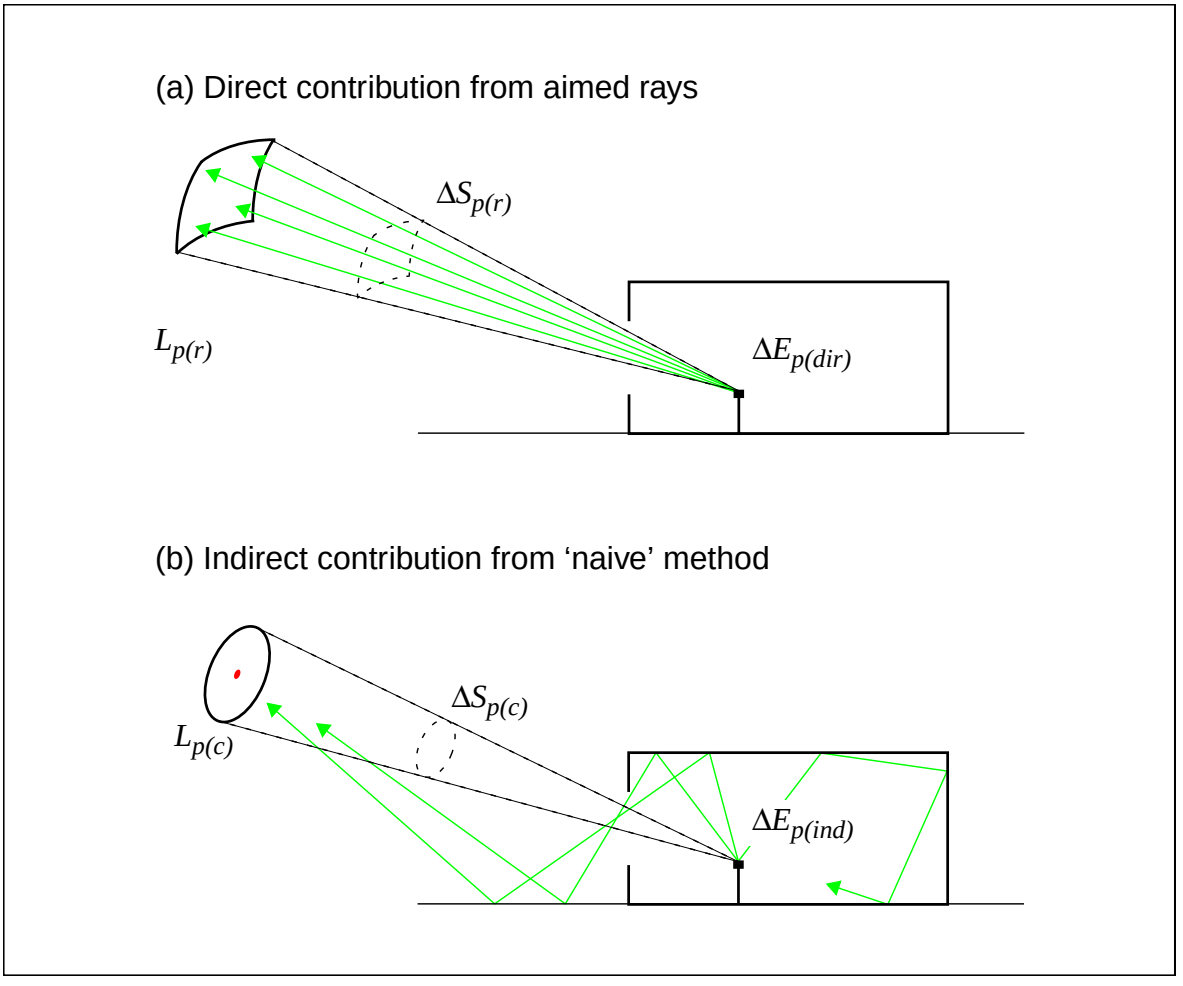

Figure 6-12. The refined formulation

Many rays are used to sample each 'rectangular' patch for the direct component. The indirect component is evaluated using the same light sources as the NM.

The DCM for the indirect component was calculated using the same technique as the Naive Method. The total and direct components for the NM were given in Figure 6-7. The indirect component therefore is simply the total minus the direct component, Figure 6-12(b). By using the NM for the indirect component, will not the DCM for this component be prone to the same errors that were identified for the direct component? Yes, however

7. With so many points distributed over the hemisphere, the sun displacement angle - the angle between the actual sun position and the nearest point on the sky vault - would be tiny. Although, for practical purposes, a DCM of size 100,366 by 6 is likely to prove unnecessarily large.

single-ray light source sampling errors are likely to be less of a problem here precisely because the indirect component is calculated using *many* rays from many different ray origins.[8] Furthermore, as discussed earlier with respect to the sun displacement angle, the indirect component is less directional in nature than the direct component. Thus the difference between a point and patch indirect DC is not likely to be so significant.

Default Refined Method DCs: Results and Analysis

The DCMs for the direct and indirect components are given in Figure 6-13. As with the total DCMs calculated using the Naive Method (Figure 6-7), these DCs exhibit a large range in magnitude: from 1.69e-5 to 0.46. For the direct DCs, it is apparent that the Refined Method has taken account of the partial occlusion of the (rectangular) sky patches. The pattern in the (non-zero) direct DCs has a coarse likeness to the image of the glazing as it would be seen in a (hemispherical fish-eye) view from the photocell location.[9] The direct DCs cover approximately 2 orders of magnitude: from 0.006 to 0.46.

The patterns for the indirect DCs, since they result from one or more reflections and do not include a direct component, are more complex. They also cover a larger range; approximately 4 orders of magnitude (1.69E-05 to 0.23). Because they were computed using a large number of reflections, all the indirect DCs have a magnitude greater than zero. The lowest altitude patches 'behind' the office, i.e. patch numbers 26-30 and 1-10 (see Figure 6-5 for key), had the smallest indirect DCs because illumination from these patches required several reflections to reach a photocell location. The

8. An approach to calculate the indirect component from 'rectangular' patches of sky was also evaluated. For this it was necessary to use a **`glow`** source hemisphere in conjunction with a *Radiance* **cal** file to modify the luminous output of the sky according to the azimuth and altitude of 'intersecting' rays. In this way, a 'rectangular' patch of sky could be made luminous, and the rest of the hemisphere set to zero. Whatever benefits there may have been in terms of complete sky coverage and many-rays sampling, they were not realised because the calculation was extremely inefficient. This was because the calculation now had to 'find' the source of (indirect) illumination - the sky patch - using Monte-Carlo sampling. In doing so, most of the (hemispherical) sampling rays were wasted because all but a small patch of the hemisphere had zero luminance.

9. See Figure 4-17 for renderings of the photocell's 'view of the glazing.

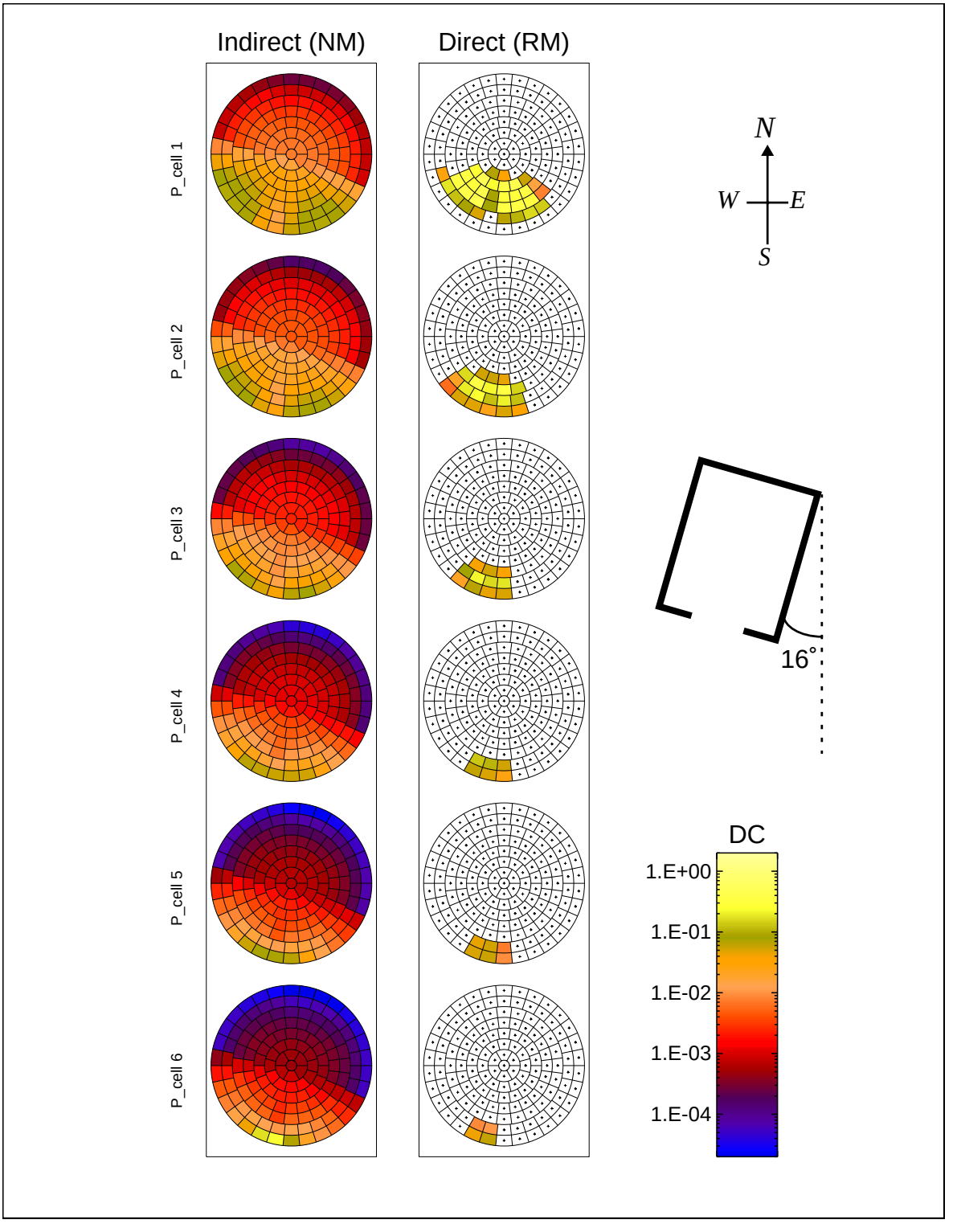

Figure 6-13. Calculated daylight coefficients for the default Refined Method

largest indirect DCs are where a photocell received, from a patch of sky, the greatest indirect illumination. The direct DCs were dependent on the visibility of the sky patch, whereas the indirect DCs were dependent on the view of those surfaces in the office that were strongly illuminated by a sky patch. The largest indirect DCs were those predicted for patches 17 and 18, for the photocell at the *back* of the office. This may at first seem counter intuitive, since it is quite rightly taken that illumination at the back of a room will always be less than at the front. Indirect DCs however, do not have an obvious relation to total illuminance.

Visualisation techniques can be used to help understand difficult illumination problems (Section 2.6.2). The complex relation between the patch position, the photocell location and the magnitude of the predicted indirect DC can be appreciated by considering, for a few cases, the photocell's 'view' of the illuminated scene. A pair of renderings generated from the viewpoint of p_cells 5 and 6 shows each photocell's view of the luminous environment when illuminated by 'circular' patch #17, Figure 6-14. The images were generated using only the direct light source calculation. It was necessary therefore to apply a small constant ambient value to make the non-directly illuminated room surfaces visible. In both renderings, the same room surfaces as seen from slightly different viewpoints are visible. These surfaces are:

- Ceiling - in shade - colour dark gray.
- Walls and window frames in shade - colour medium gray.
- North wall - strong illumination - colour white (top on image).
- West wall - 'low' illumination - colour light gray (right of image).

The light source in this projection is just visible through the South facing window.[10] The centre of the 'circular' light source #17 was at altitude 6˚ and

10. Although the light source appears as a disc in the image, all surface-to-source light transfer is modelled using a single ray aimed towards the source centre.

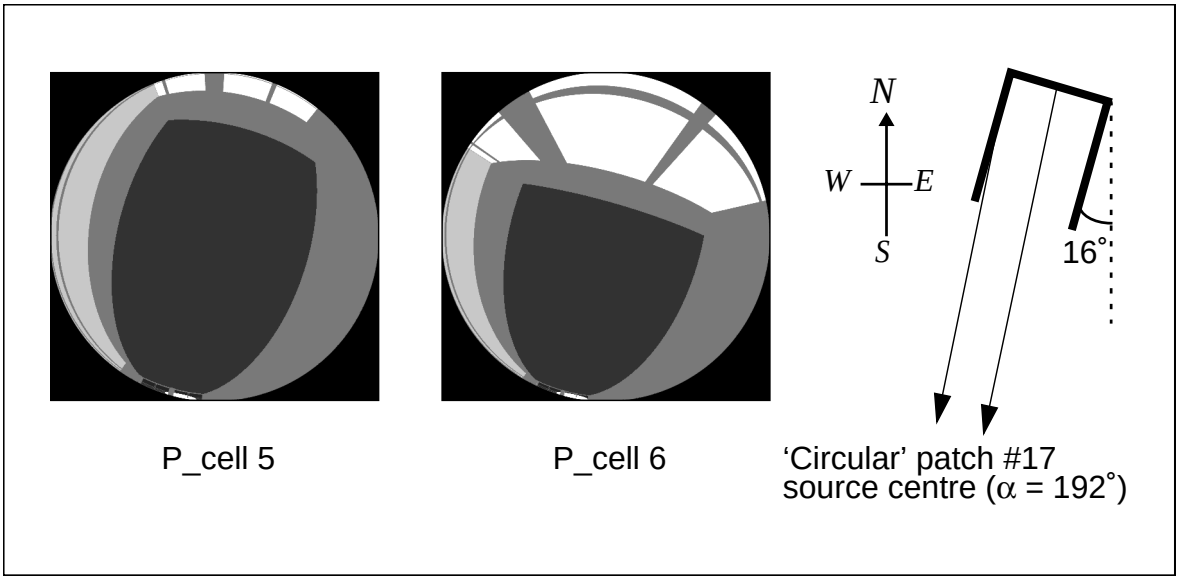

Figure 6-14. Photocell hemispherical views for scene illuminated by patch# 17

These renderings have been laterally inverted West - East to relate to the compass orientated DC plots.

azimuth 192˚. The outgoing surface normal from the glazing has an azimuth of 196˚. Light from the source therefore 'shines' down the length of the room, illuminating the North wall at close to normal incidence. The luminance of the directly illuminated part of the North wall was ~10 times that of the West wall where the source angle of incidence was close to grazing i.e. just < 90˚, Figure 6-14. It is readily apparent from the renderings that p_cell 5 'sees' much less of the bright rear wall than does p_cell 6. The hemispherical view used for these fish-eye images contains a cosine weighting of the (hemisphere) projected solid angle. For illumination therefore, equal areas of equal luminance (in the field of view) contribute equally to the total illuminance at the viewpoint. As a consequence, the indirect DC for patch #17 was greater at p_cell 6 than at p_cell 5. For a multiple-reflection indirect calculation, most if not all of the internal surfaces will attain some non-zero luminance value. It was the first reflection however, from the photocell to the source that provided the greatest contribution to the indirect illuminance. Note also from these renderings the effect of single-ray light-source sampling - no penumbras. As a consequence, the East wall was not

illuminated by the light source, even though the edge of the circular source (patch) was just visible from the wall surface.[11]

The two methods: a simple test

The potential for error associated with the Naive Method is revealed in the following tests. The direct component of illuminance from a uniform luminance sky was derived from daylight coefficients predicted using both the Naive and Refined methods. These were compared against the illuminance predicted using the standard calculation for the same sky. The results are shown in Figure 6-15(a).

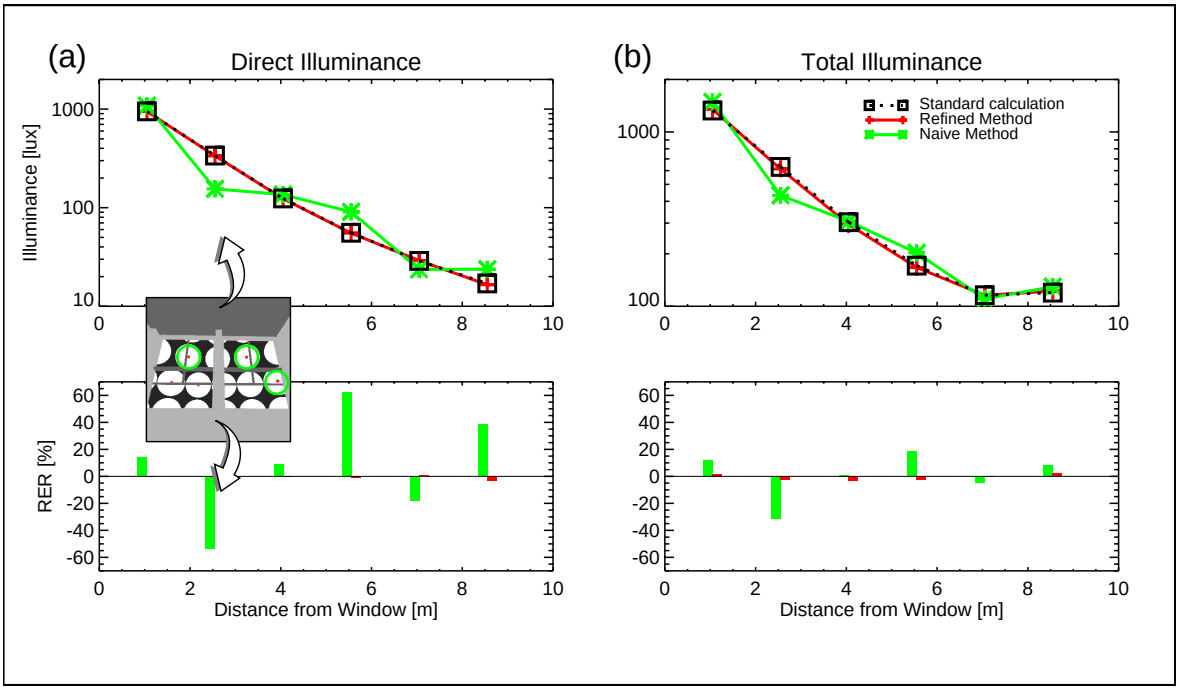

Figure 6-15. NM and RM comparison test

Inset rendering shows the 'view' from p_cell 2 of the NM sky patches. The centres of only three patches are visible (❍), resulting in marked under-prediction of the direct component.

11. Consider, the angle of incidence of the source centre to the (internal) East wall was 94˚, and so not visible. However a tiny segment of the 11˚ source-angle, just 1.5˚, was visible from the East wall.

For this test, the accuracy of the standard calculation was not an issue, the illuminance values predicted using this method should, for the purpose of comparison, be considered correct.[12] Thus, the relative error in the DC derived predictions is shown with respect to the standard calculation. For the direct component, it is clear that the NM performed poorly with erratic behaviour across the six photocells. The relative errors range from about -55% (p_cell 2) to about +55% (p_cell 4). The Refined Method predictions however are barely distinguishable from those for the standard calculation.

The standard calculation was repeated to predict the total illumination from the uniform sky. The results from the validation of the standard calculation (Chapter 4) showed that, when the circumsolar luminance was not an issue, the internal illuminance was predicted to a high degree of accuracy. Thus for a uniform luminance sky, the standard calculation predictions are considered to be correct. The total illuminances (i.e. direct plus indirect component) derived using each Method were compared against predictions using the standard calculation, Figure 6-15(b). Here, the errors for the NM were less than for the direct-only component. But nevertheless significant, particularly for p_cell2 where the relative error was about -30%. These two tests offer only indications of the degree of inaccuracy that might be expected using the Naive Method because, of course, real skies have non-uniform luminance distributions. The test however was sufficient to demonstrate that the Refined Method was a superior technique.

6.2.5 The 'Finescale Refined Method'

It was suggested in Section 6.2.4 that imprecision resulting from single ray light source sampling is likely to be much less significant for the indirect component than for the direct. This assertion is now re-examined following the investigation of the cause for the high-value indirect DC for patch# 17 at p_cell 6 (Figure 6-13 and Figure 6-14). It was shown that, for this patch-

12. The reliability of the standard illuminance was ensured by increasing the number of hemispherical sampling rays until satisfactory convergence had been achieved at all photocell locations.

photocell combination, the indirect DC was in fact highly directional in nature. Thus, small displacements in the patch centre could have resulted in marked changes for the magnitude of the indirect DC. It is conceivable therefore that, at the Default discretisation (N_{patch} = 145), the indirect DCM may contain imprecisions resulting from single-ray light-source sampling. Albeit for only a small number of patches. To test if this was a significant effect, the indirect DCM was evaluated using a finer discretisation. Called the 'Finescale' discretisation, this scheme used four evenly spaced 5° light source solid angles (i.e. patches) for each patch of the Default scheme, Figure 6-16. This gave a total of 580 patches for the 'Finescale' indirect DCM, and so it required four times longer to compute than the 'Default' indirect DCM.

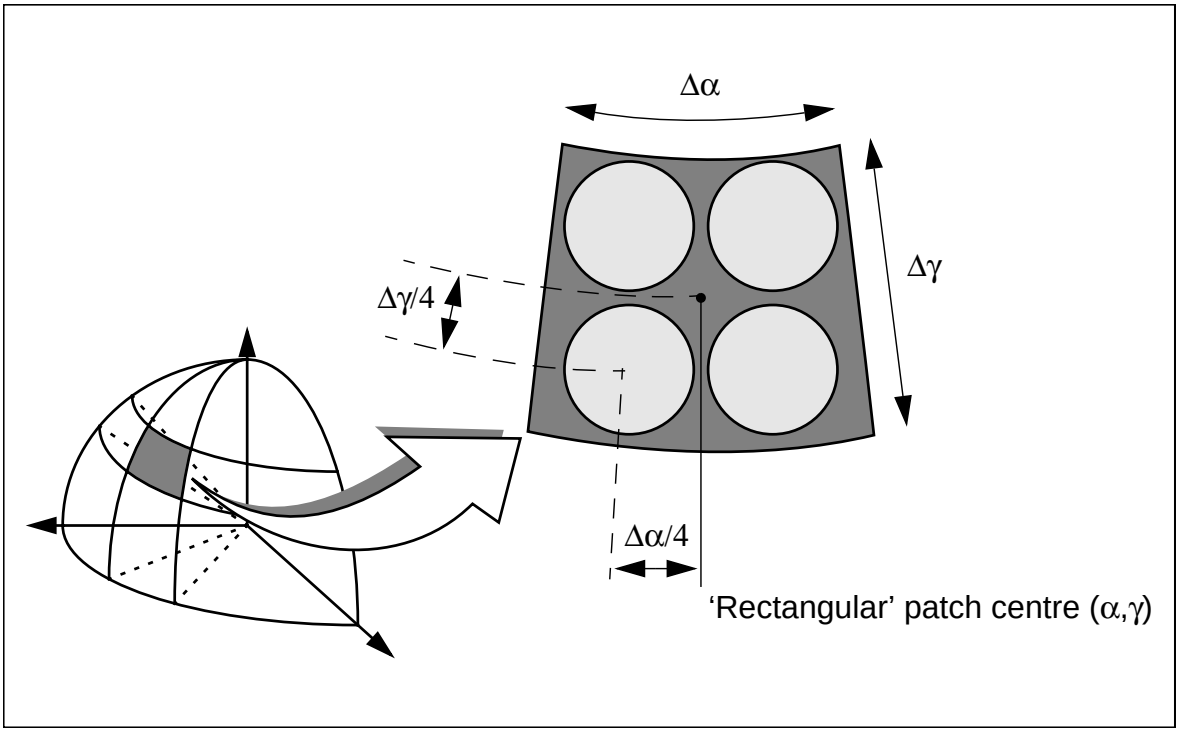

Figure 6-16. Four 'finescale' patches for each 'default' patch

Finescale Refined Method DCs: Results and Analysis

The intention here is to discover significant differences, if any, between the Finescale and Default discretisations for the indirect DCM. And, if significant differences are found, to anticipate their consequences for illuminance prediction. The method for doing this was as follows. If there was little variation in the DCs within each group of four finescale patches, it was assumed that they would have a similar illumination effect to the single default patch. This was a reasonable assumption for the patch configurations considered here. Indirect DCs can be highly sensitive to the source's angle of incidence on the principal internal surfaces (i.e. walls, floor and ceiling). This is apparent from Figure 6-14 where a small clockwise shift in azimuth for patch 17 would switch the illumination from the West wall to the East wall.

What follows is a three stage graphical analysis. Results are shown for photocells 1 and 6 only to reduce the number of plots, Figure 6-17. Firstly, the two plots at the top show the indirect DCMs at the two photocell locations. In terms of shade and pattern, the DCMs for the 'Finescale' scheme appear very similar to those for the 'Default' (Figure 6-13). It is possible however to discern variation in the magnitude of the indirect DC within some groups of four from shade alone. The difference in DCs within each group of four is better revealed as a coefficient of variation. These are the two plots in the middle of Figure 6-17. The coefficient of variation (CoV), for any group of four patches, is simply the variance of the group divided by the mean, i.e.

$$CoV = \left(\frac{\sum_{j=1}^{4} (DC_j - \overline{DC})^2}{4-1} \right) / \overline{DC} \qquad \textbf{(6-17)}$$

Here the range in CoV varies from low (0 to 0.05), indicated by a blue shade, to high (> 0.25), indicated by pink. Below these are plots of the normalised coefficient of variation (NCoV) which will be discussed later.

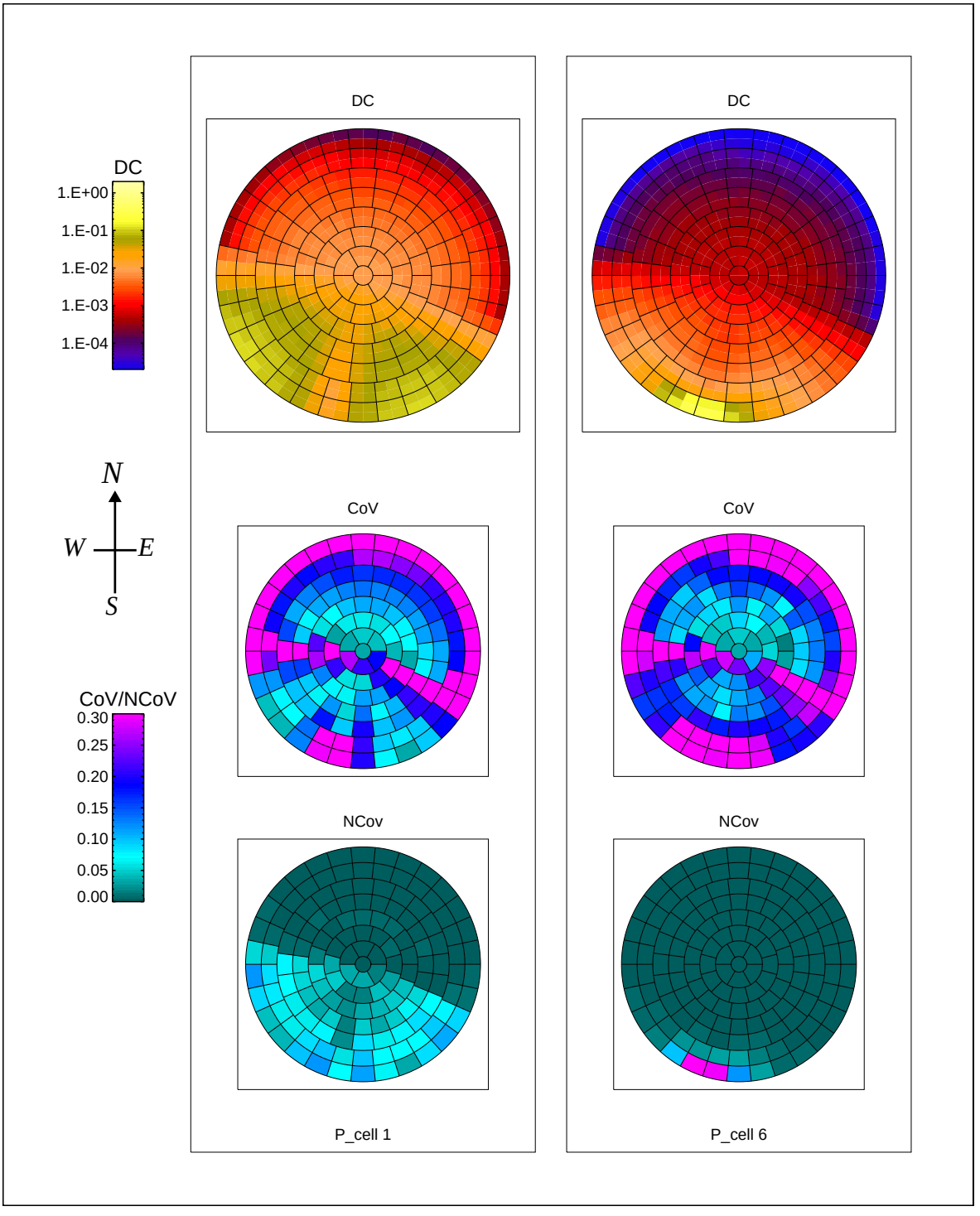

Figure 6-17. Indirect DCMs for the finescale discretisation at p_cells 1 and 6

The top two plots show the magnitude of the indirect DCs for the 580 patches. The middle two plots show the coefficient of variation (CoV) within each group of four patches. The bottom two plots show the normalised coefficient of variation (NCoV).

Returning now to the patterns in the CoV. These patterns can be related to the scene geometry. Re-plotting the CoV graphic for p_cell 6 alongside a schematic of the room shows this more clearly, Figure 6-18.

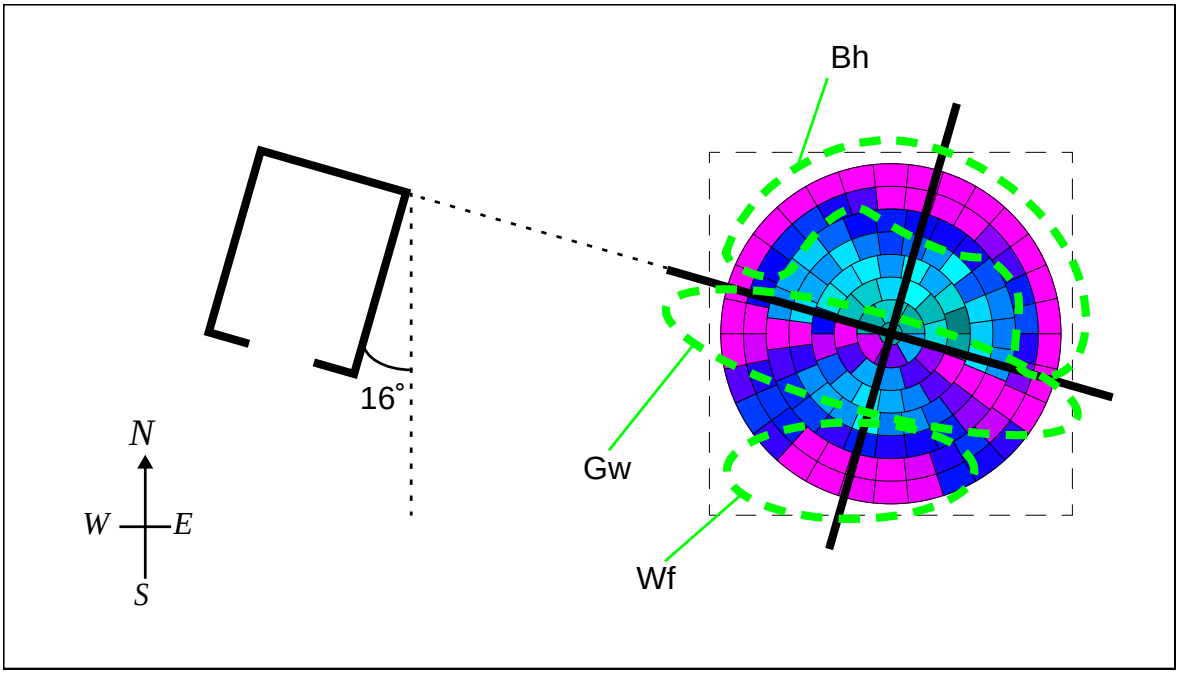

Figure 6-18. Relationship between the building configuration and the spatial pattern in the coefficient of variation for p_cell 6

Three distinct regions of high (pink) CoV are delineated. They are labelled as follows:

- Wf - showing patches which are, from the photocell viewpoint, visible through the window, or just outside the field of view.
- Gw - here the stripling of pink (i.e. high) CoV values shows those patches which have a near grazing incidence to the office window.
- Bh - this indicates the arc of patches that were “behind” the office-room and just above the horizon.

The appearance of these three regions of high CoV can be explained by considering what effect a small displacement in source position has on the resulting indirect illuminance at the rear of the room.

Consider first the patches in the region marked Wf. Recall the view from p_cell 6 as shown in Figure 6-14. In that image, the scene was illuminated by sky patch #17 - one of those patches which when subdivided appears here in region Wf. It is clear from this view that small (~5˚) displacements in source position have a significant effect on scene illumination.

The high CoV patches within the region Gw clearly show a relationship with the plane of the glazing. This is to be expected since small displacements in source position will have a twofold effect on room illumination. At close to grazing incidence, say 10˚, a change to 5˚ will greatly reduce both the projected area of illumination inside the room and the transmission of light through the glazing.

Those patches behind the office-room, region Bh, cannot illuminate the space directly - at least one reflection of light from the ground plane "up" into the room is required. So it is the luminance of the ground plane, lit by a source patch, that determines the resulting illuminance inside the space. Therefore, for patches (within a group of four) just above the horizon, two will be at altitude 3˚, and two at 9˚. The ground plane luminance due to the higher altitude patches will be $(\sin 9^\circ / \sin 3^\circ) \approx 3$ times brighter than for the lower altitude patches. Thus the patches at higher altitude will yield a higher indirect DC - see Figure 6-17 for verification of this.

Returning now to the plots of the NCoV (bottom of Figure 6-17). The NCoV is the CoV multiplied by a normalisation factor:

$$NCoV = CoV \times \overline{DC} / \overline{DC}_{max} \qquad \textbf{(6-18)}$$

where $\overline{DC}_{max}$ was the maximum of the 145 values of $\overline{DC}$ at each photocell. A high NCoV (pink) therefore discloses those sectors where both the CoV was high *and* where the mean indirect DC was large. Although there was a high CoV in the group of four DCs for both p_cell1 and p_cell6, only for patches 17 and 18 at p_cell6 was the NCoV comparably large. This suggests that, if there is a difference in the derived illuminance predictions between the Default and Finescale discretisations, the difference will be more

noticeable at p_cell6 than at p_cell1, and it will be due to those patches that had a high NCoV.

6.3 Validation of DC derived illuminances

6.3.1 DC formulation for validation

The illuminance at a photocell location, *E*, was evaluated as the sum of four illuminance components:

$$E = E^{d} + E^{i} + E^{sd} + E^{si} \quad \textbf{(6-19)}$$

Where E^{d} and E^{i} are, respectively, the direct and indirect components of illuminance due to the sky. Similarly, E^{sd} and E^{si} are the direct and indirect components of illuminance due to the sun. The illuminance components E^{d}, E^{i} and E^{si} were derived from the DCMs computed using variants of the 'Refined Method', Figure 6-19. For the purpose of validation, the direct sun component was determined using the standard calculation. The DC derived illuminance predictions were partitioned in the same way as for the standard calculation (Section 4.5). Accordingly, all the instances where the sun was visible from the photocell location (i.e. $E^{sd} > 0$) were classed as potentially unreliable and eliminated. Thus the validation results were insensitive to the magnitude of the direct sun component and any value could have been used. The way the direct sun illuminance should be calculated in a generalised DC scheme is discussed later.

The direct components of illuminance account for window and room configuration, external obstructions and glazing transmittance. The indirect quantities account for the inter-reflected light components, which for both cases, sun and sky, include internal and external reflections. In contrast to the scheme described by Littlefair [92], the illuminance components used here are defined by type - direct or indirect - and luminous origin - sun or sky. All the external obstructions and reflections etc. are absorbed in these four categories.

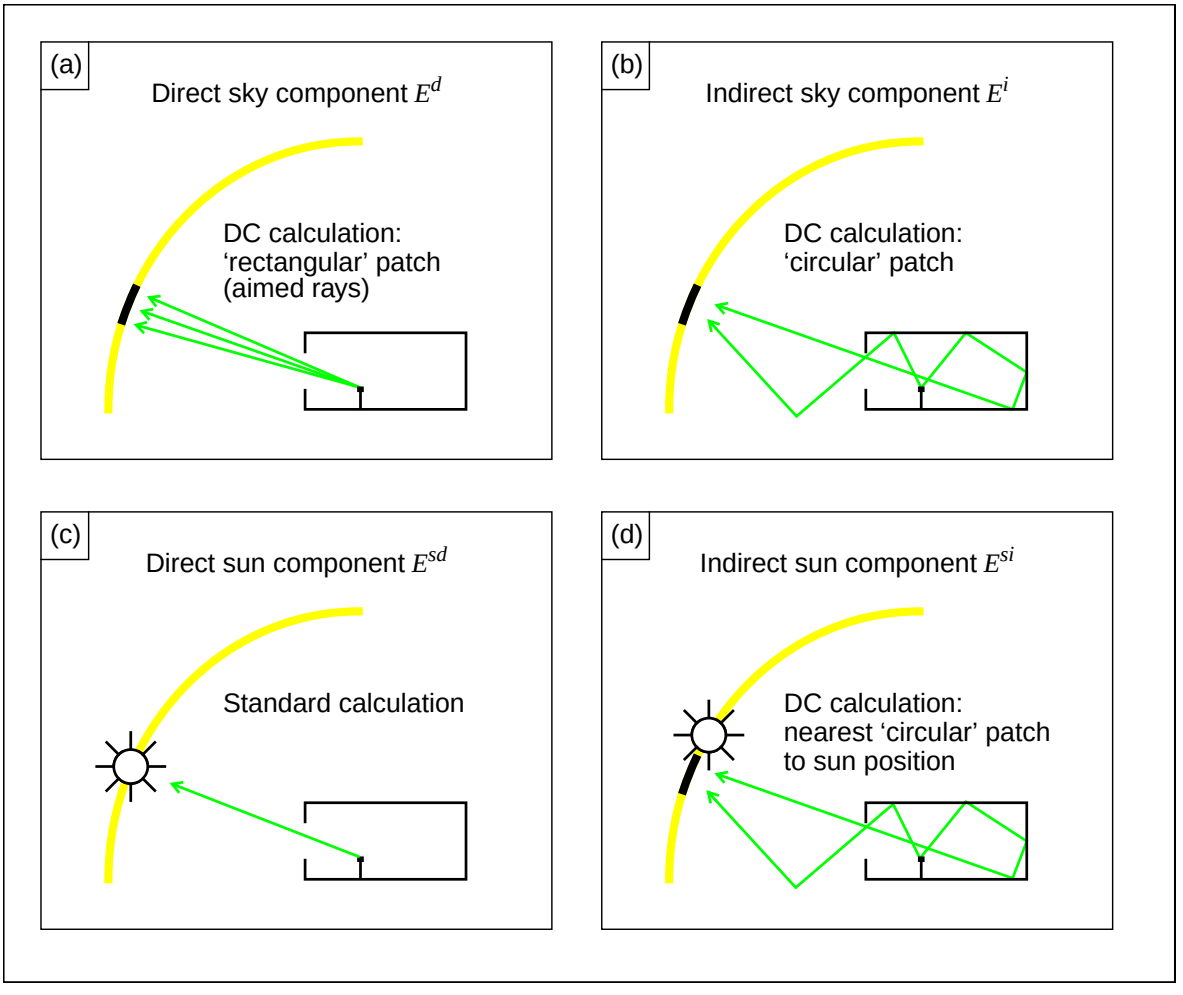

Figure 6-19. The four components of illumination

The components of illumination due to skylight

The illumination from skylight was derived from (*m* x *n)* daylight coefficient matrices for:

- the direct sky component $\mathbf{D}^d$ (Refined Method), and
- the indirect sky component $\mathbf{D}^i$ (Naive Method).

Where *m* was the number of points in the office (i.e. photocell locations) and *n* was the number of sky patches.

The skylight only illumination (no sun) is the sum of the direct and the indirect illumination

$$\mathbf{E}^{sky} = \mathbf{E}^{d} + \mathbf{E}^{i} \tag{6-20}$$

where

$$\mathbf{E}^{d} = \mathbf{D}^{d} \times \mathbf{c} \tag{6-21}$$

and

$$\mathbf{E}^{i} = \mathbf{D}^{i} \times \mathbf{c} \tag{6-22}$$

Giving the illuminance vector for skylight in terms of DCMs as

$$\begin{aligned} \mathbf{E}^{sky} &= (\mathbf{D}^{d} \times \mathbf{c}) + (\mathbf{D}^{i} \times \mathbf{c}) \\ &= (\mathbf{D}^{d} + \mathbf{D}^{i}) \times \mathbf{c} \end{aligned} \tag{6-23}$$

The *n* element column vector **c** is formed from the product of the solid angle and the luminance for the sky patches.

The solar components of illumination

As noted above, the direct component of illuminance due to the sun, $\mathbf{E}^{sd}$, was determined using the standard calculation - although the outcome of the validation is insensitive to this value. The indirect component of illumination from sunlight, $\mathbf{E}^{si}$, was evaluated using part of the daylight coefficient matrix for indirect sky illumination, $\mathbf{D}^{i}$, such that

$$\mathbf{E}^{si} = \mathbf{D}^{i}_{\beta} S^{sun} L^{sun} \tag{6-24}$$

Where $\mathbf{D}^{i}_{\beta}$ is column β of the $(m \times n)$ matrix $\mathbf{D}^{i}$ for the (indirect) patch nearest to the sun position.[13] The scalars S^{sun} and L^{sun} are, respectively, the solid angle and the luminance of the sun.

13. For any given sun position, the angle between the sun and every indirect patch was calculated, and the nearest indirect patch to the solar position, represented by the index β, was identified.

The total illuminance due to the sun is the sum of the direct and the indirect components

$$\mathbf{E}^{sun} = \mathbf{E}^{sd} + \mathbf{E}^{si} \tag{6-25}$$

which, in terms of the column vector extracted from the DCM for the indirect sky component, is:

$$\mathbf{E}^{sun} = \mathbf{E}^{sd} + \mathbf{D}^{i}_{\beta} S^{sun} L^{sun} \tag{6-26}$$

Total illuminance in terms of DCMs

The *m* element vector for the internal illuminance, **E**, is

$$\mathbf{E} = (\mathbf{D}^{d} \times \mathbf{c}) + (\mathbf{D}^{i} \times \mathbf{c}) + \mathbf{E}^{sd} + \mathbf{D}^{i}_{\beta} S^{sun} L^{sun} \tag{6-27}$$

This is the 'kernel' form of the daylight coefficient equation that was used for this study. Variants of this equation are described in the following section.

6.3.2 Variants of the daylight coefficient formulation

The Default and Finescale indirect DCMs are referred to, respectively as, $\mathbf{D}^{i145}$ and $\mathbf{D}^{i580}$. Likewise, the vector, **c**, formed from the product of sky patch solid angle and luminance, contains 145 elements in the Default scheme ($\mathbf{c}^{145}$) and 580 elements for the Finescale discretisation ($\mathbf{c}^{580}$). The direct sky component DCM $\mathbf{D}^{d}$ was the same for all variants i.e. n = 145. The equations for the four variants are given below.

Variant 1

This is simply the default formulation.

$$\begin{aligned} \mathbf{E} &= (\mathbf{D}^{d} \times \mathbf{c}^{145}) + (\mathbf{D}^{i145} \times \mathbf{c}^{145}) + \mathbf{E}^{sd} + \mathbf{D}^{i145}_{\beta} S^{sun} L^{sun} \\ &= (\mathbf{D}^{d} + \mathbf{D}^{i145}) \times \mathbf{c}^{145} + \mathbf{E}^{sd} + \mathbf{D}^{i145}_{\beta} S^{sun} L^{sun} \end{aligned} \tag{6-28}$$

Variant 2

This formulation used the Finescale discretisation to evaluate the indirect component of illumination from the sky.

$$\mathbf{E} = (\mathbf{D}^{d} \times \mathbf{c}^{145}) + (\mathbf{D}^{i580} \times \mathbf{c}^{580}) + \mathbf{E}^{sd} + \mathbf{D}_{\beta}^{i145} S^{sun} L^{sun} \quad \textbf{(6-29)}$$

Variant 3

Here the Finescale discretisation was used to evaluate the indirect component of illumination from the sun.

$$\begin{aligned} \mathbf{E} &= (\mathbf{D}^{d} \times \mathbf{c}^{145}) + (\mathbf{D}^{i145} \times \mathbf{c}^{145}) + \mathbf{E}^{sd} + \mathbf{D}_{\beta}^{i580} S^{sun} L^{sun} \\ &= (\mathbf{D}^{d} + \mathbf{D}^{i145}) \times \mathbf{c}^{145} + \mathbf{E}^{sd} + \mathbf{D}_{\beta}^{i580} S^{sun} L^{sun} \end{aligned} \quad \textbf{(6-30)}$$

Variant 4

This last variant used the Finescale discretisation to calculate the indirect component of both the sun and the sky illumination.

$$\mathbf{E} = (\mathbf{D}^{d} \times \mathbf{c}^{145}) + (\mathbf{D}^{i580} \times \mathbf{c}^{580}) + \mathbf{E}^{sd} + \mathbf{D}_{\beta}^{i580} S^{sun} L^{sun} \quad \textbf{(6-31)}$$

The variants are summarised in Table 6-1.

	Sky component		**Sun Component**	
Variant	**Direct**	**Indirect**	**Direct**	**Indirect (sky)**
1	Refined Method (aimed rays)	Default	Standard calculation	Default
2		Finescale		Default
3		Default		Finescale
4		Finescale		Finescale

Table 6-1. DC Variants

6.3.3 Pre-process of the sky luminance measurements

The conversion of the sky luminance data to a suitable format for the standard calculation was described in Section 3.2.5. The conversion for the validation of the DC derived illuminances required a similar process, except that in this instance, the pattern for the interpolated sky luminance data was identical to the pattern for the measurement. The daylight coefficient

implementation required a sky vault discretisation that was based on a fixed-orientation pattern, whereas the orientation for the measured pattern was variable, Figure 6-20. Apart from these differences, the interpolation of

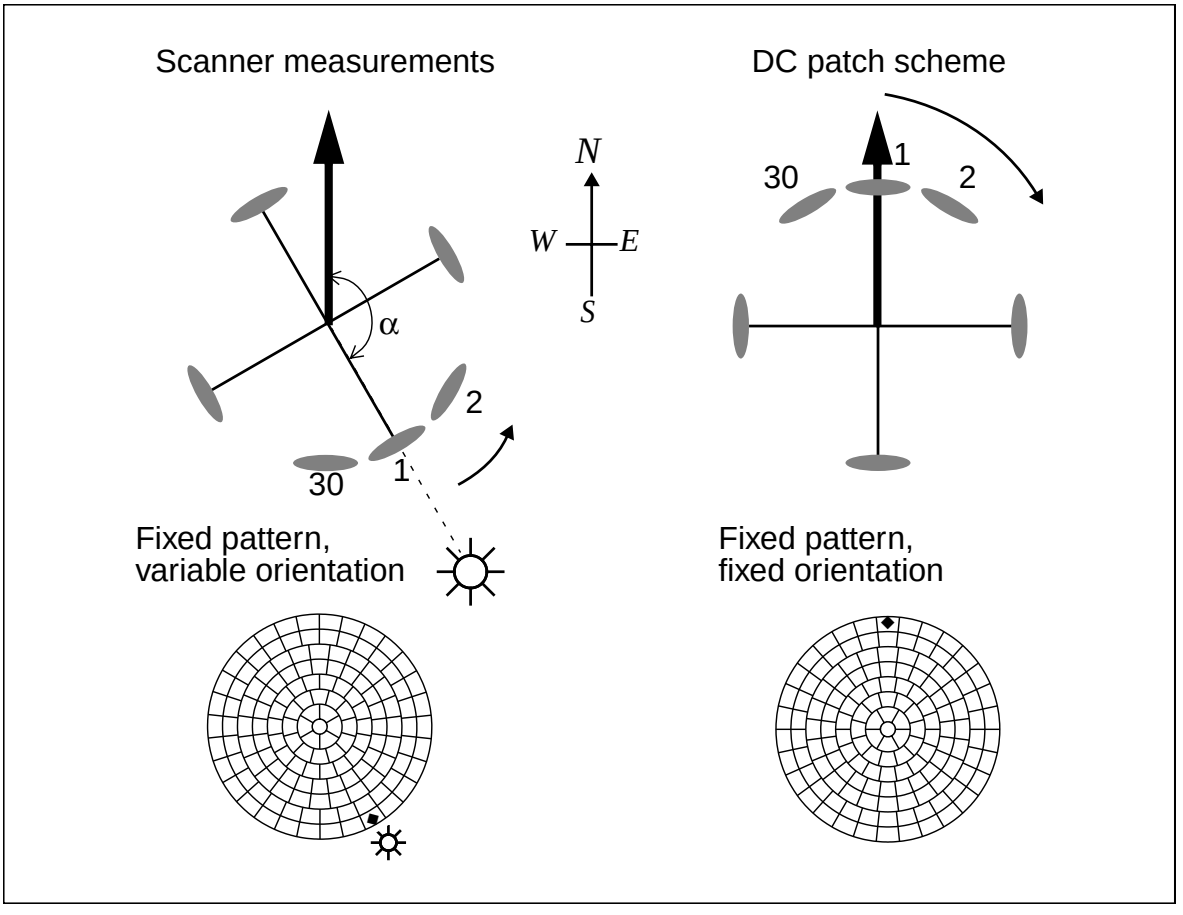

Figure 6-20. Comparison of scanner measurement pattern with DC patch scheme

the measurement pattern to the DC pattern and normalisation of the sky luminance used the techniques described in Section 3.2.5. An example of a measured and interpolated sky for use with daylight coefficients is given in Figure 6-21. This same sky (125_92_13h15) was given as an example of the interpolation applied for the standard calculation (Figure 3-20). The differences between that interpolation and the one shown in Figure 6-21 are slight; in both cases it is likely that the circumsolar sky luminance was underestimated.

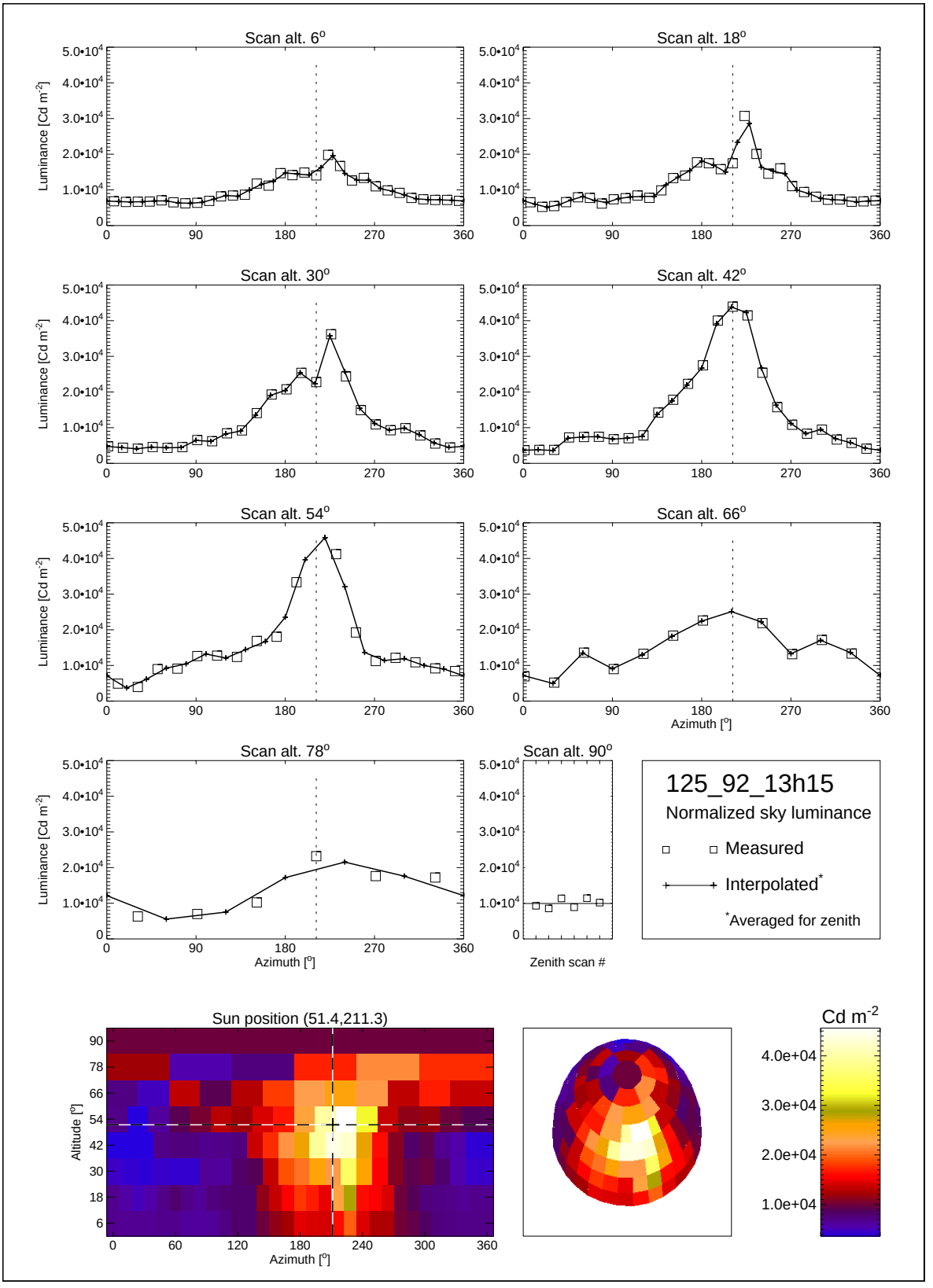

Figure 6-21. Sky 125_92_13h15

6.3.4 Results

Illuminance predictions for the 754 skies in the BRE-IDMP validation dataset were derived using the four DC variants (Eq 6-28 to Eq 6-31). As with the standard calculation, the predictions were partitioned into 'reliable' and 'unreliable' sets according to the visibility of the 6˚ circumsolar region (Section 4.5). Only those photocell-scan combinations classed as reliable were used for comparison with measurements and the predictions using the standard calculation.

The overall mean bias error (MBE) and root mean square errors (RMSE) for the illuminance predictions at each photocell for the standard calculation and the four variants of the daylight coefficient implementation are shown in Figure 6-22. The number of reliable photocell-scan combinations is marked at each photocell position, i.e. N_{scan} = 688 for photocell 4.

The illuminance predictions from the standard calculation were generally better than those for any of the DC variants, particularly in terms of MBE for those photocells at the back of the room. The differences from the measurements were however not that great, and the MBEs for DC variants 2 and 4 were always less than 10% for all photocells.[14] The differences in prediction between the four DC variants were significant only at the back of the room (p_cells 5 and 6). It was suggested in Section 6.2.5 that this was likely to be the case. Even so, the differences were not that large. Variant 2 performed marginally better than Variant 3. This suggests that, for the skies in the validation dataset, the indirect sky component was more sensitive to the change in patch discretisation (Default to Finescale) than the indirect sun component. Variant 4 performed the best, but the improvement over Variant 2 was only marginal.

14. With the exception of photocell 3, which may contain a calibration error (Section 4.5.3).

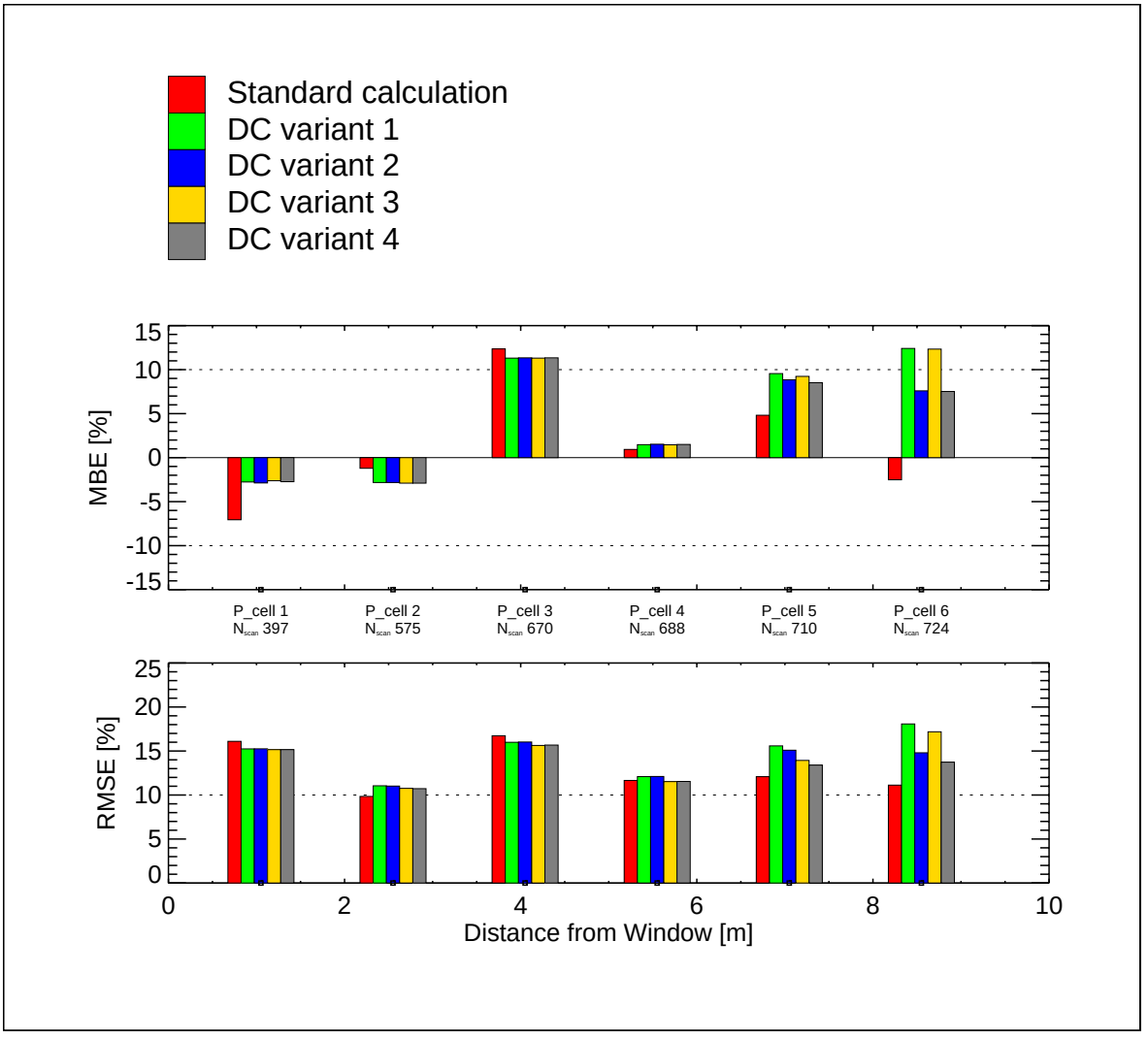

Figure 6-22. Error characteristics for the 4 DC variants and the standard calculation

Time-series plots for DC variant 4 and the standard calculation

The relative error in the illuminance prediction for daylight coefficient variant 4 (DCV4) and the standard calculation is shown with the corresponding time-series for global horizontal, diffuse horizontal and vertical South illuminance in Figure 6-23 to Figure 6-26. These plots use the same format as in earlier chapters. Only those photocell-scan combinations that were classed as reliable are shown. The relative error in DCV4 predictions is marked by blue (■) square, and the standard calculation by a red (■) square. There are 27 pairs of plots in the figures: one for each day in the validation dataset.

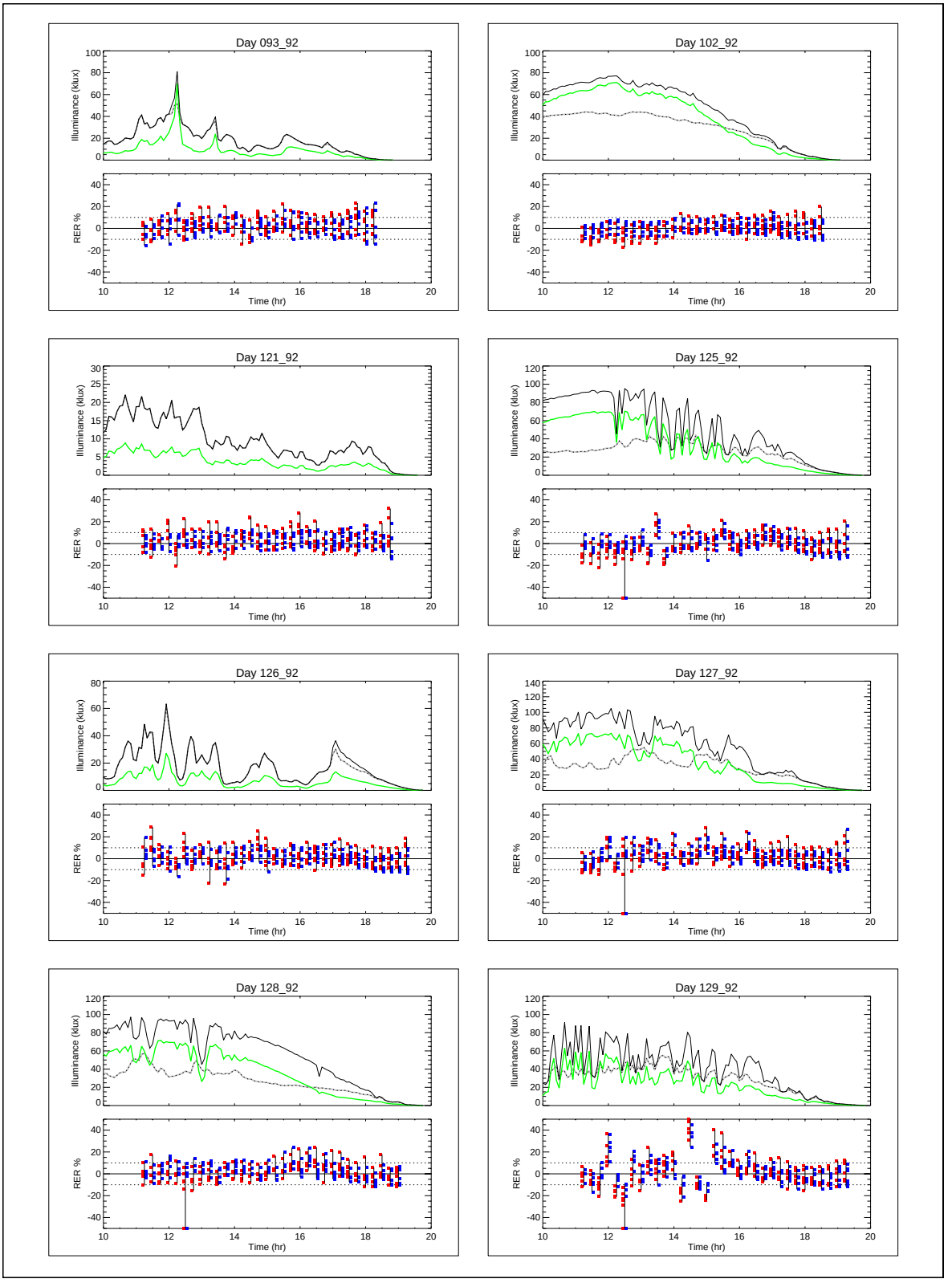

Figure 6-23. Comparison standard calculation and DC variant 4

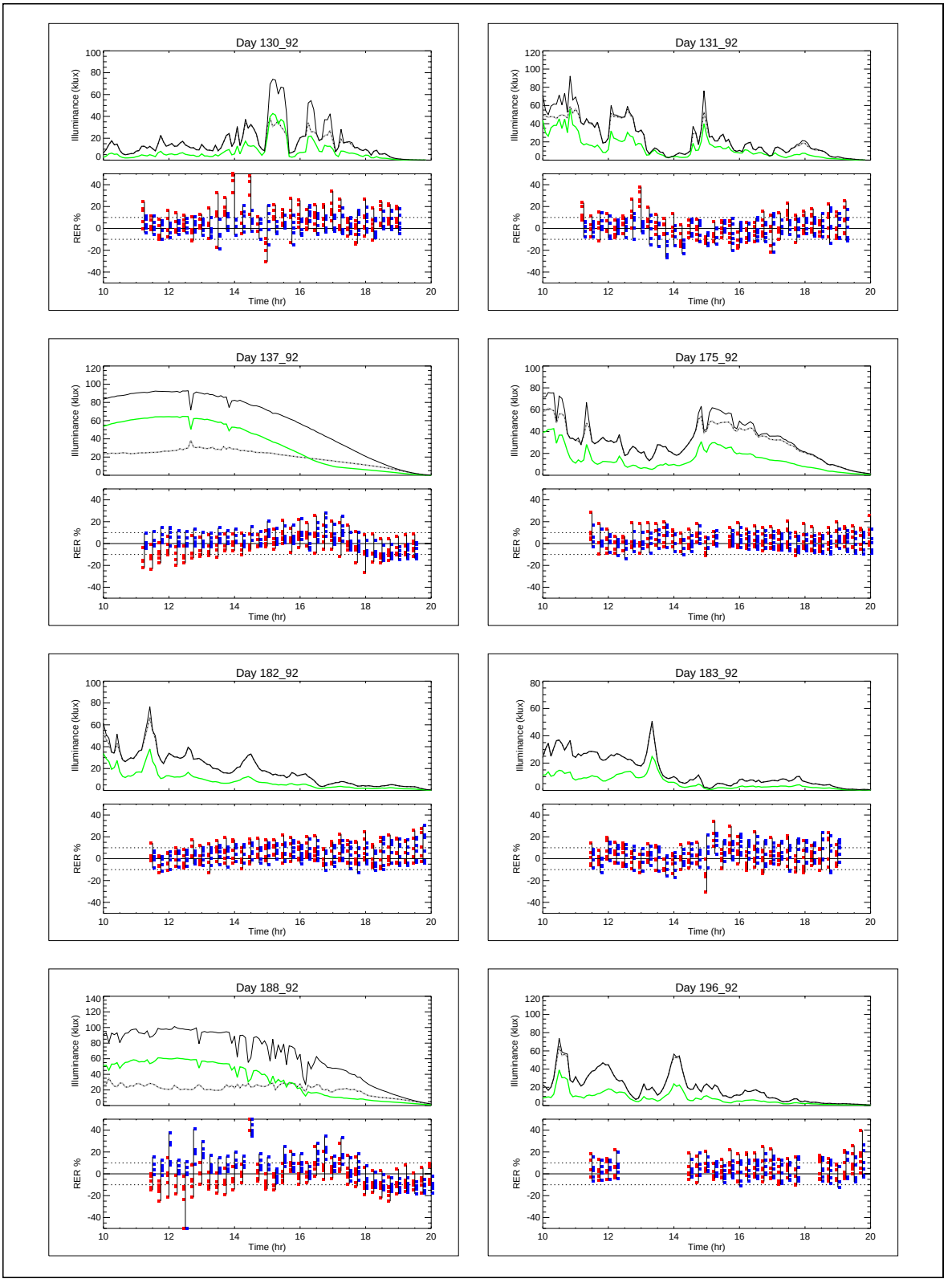

Figure 6-24. Comparison standard calculation and DC variant 4

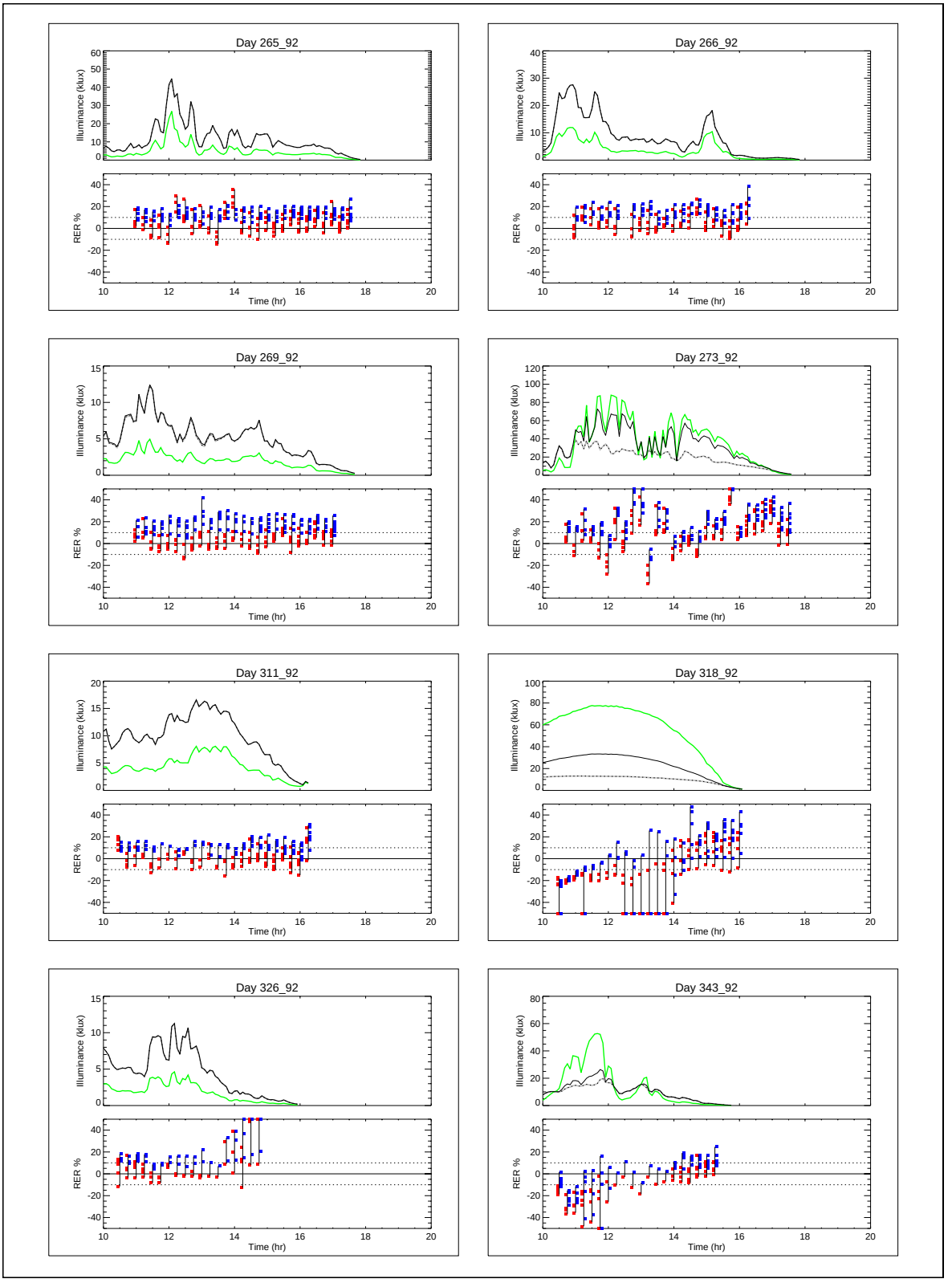

Figure 6-25. Comparison standard calculation and DC variant 4

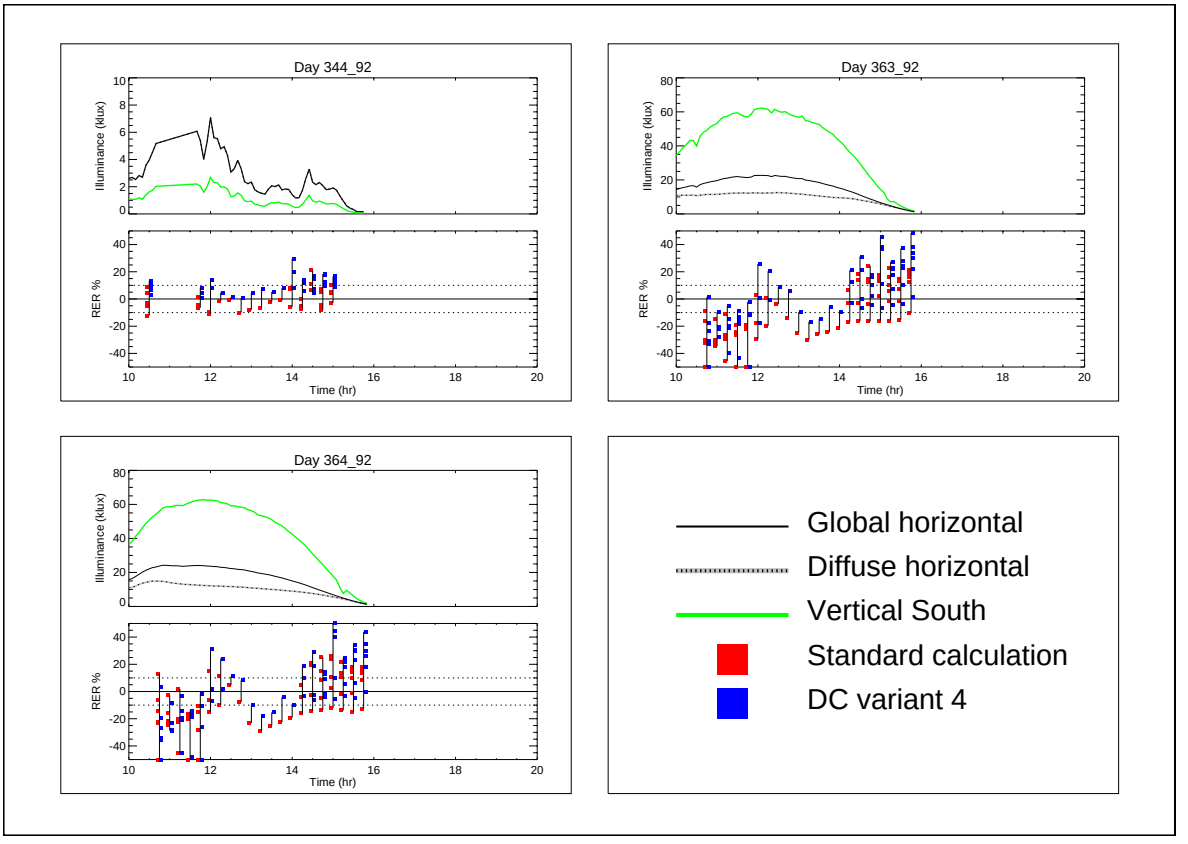

Figure 6-26. Comparison standard calculation and DC variant 4

From these plots, the following observations are made:

1. The RERs for DCV4 were generally good (i.e. RER < 10%).
2. The RERs for DCV4 were comparable to those obtained using the standard calculation.
3. For both DCV4 and the standard calculation, some RERs were noticeably large (> 20%) for clear sky conditions from day 273_92 onwards.
4. For overcast conditions late in the year, e.g. days 265_92, 266_92 and 269_92 (Figure 6-25), DCV4 tended to overpredict slightly in both absolute terms, and relative to the standard calculation.

The difference in performance between any of the DC variants and the standard calculation was discernible. Though for most practical purposes, the differences are not considered to be important.

6.3.5 Summary

The daylight coefficient approach has been successfully implemented using the *Radiance* system as the calculation 'engine'. The validation of the daylight coefficient derived illuminance predictions was carried out using the same rigorous procedures as for the standard calculation. The error characteristics for the daylight coefficient derived illuminances have been demonstrated to be comparable to those for the standard calculation. In the following section, a generalised daylight coefficient approach is described and demonstrated.

6.4 DC Based daylighting analysis: The way ahead

6.4.1 Background

Daylight modelling in the UK has traditionally been based on the convention of a Standard Overcast Sky for three reasons:[15]

- If the natural lighting is sufficient on an overcast day it is likely to be more than adequate when the sun is shining.
- A densely overcast sky looks the same whichever direction (in plan) one faces - north, south, east or west. The effect of the orientation vanishes from the calculation.
- Given the overall luminance profile of the Standard Overcast Sky, the illuminance at any given point indoors must be directly proportional to the simultaneous outdoor illuminance under the unobstructed overcast sky vault, whether the sky itself is bright or dull.

15. Taken from the CIBSE virtual conference pages - **http://www.virtual-conference.com/cibse97/conference/papers/e-html/DAYFAC.HTM**

It is fair to say that the approach has gained favour largely because of its simplicity rather than its intrinsic accuracy. The assumption of a CIE Standard Overcast Sky transforms what is in reality a time-varying scenario - a succession of unique sky and sun conditions - into one that is static. The penalty of simplicity however is a considerable loss in realism. It is impossible to reproduce using an overcast sky the naturally occurring variations in the quantity, the character (e.g. diffuse, direct) and the distribution of internal daylight levels.

It has long been appreciated that the ratio of internal to external illuminance varies greatly under real skies [Tregenza 83], but the significance of this has yet to be accurately quantified. For this to be achieved, realistic measures of the true long-term daylighting performance for buildings must be made. The assessment period should ideally be a full year so that the seasonal variation in daylight is captured (Figure 6-1). And the timestep at which the evaluation is carried out should be small enough to capture the observed short-term variation in daylight. The most readily available sources of data that matches these requirements are climatic or weather tapes (see Section 2.1.1). These data contain hourly integrated values for a full year. Standardised weather tapes, known as Test Reference Years, are usually based on several years data so that the effect of 'exceptional' years is minimised. The use of daylight coefficients to predict long-term daylighting performance based on Test Reference Year data is described and demonstrated in the sections that follow.

6.4.2 A system to predict time-varying illuminances

The DC Variant 1 implementation (Section 6.3.2) was generalised so that illuminances for all four components could be derived from daylight coefficients.[16] In the generalised scheme, the direct sun illuminance was derived from a direct component DCM for 5010 points evenly distributed

16. Because these are demonstration examples, the simplest DC variant was used. In practice, DCV4 would be the best one to use.

over the hemisphere. Following the procedure outlined by Littlefair (see Section 6.1.2), the basic climate data used for the all examples that follow were obtained from the Kew84 Test Reference Year. The building model for these examples was the BRE office so the daylight coefficients calculated for the validation were re-used. Only the direct DCM for the 5010 points needed to be calculated anew - a relatively trivial task taking only a few seconds to compute.The internal illuminance therefore was calculated using Eq 6-28 with the direct sun component $\mathbf{E}^{sd}$ now derived from daylight coefficients:

$$\mathbf{E} = (\mathbf{D}^{d} \times \mathbf{c}^{145}) + (\mathbf{D}^{i145} \times \mathbf{c}^{145}) + \mathbf{D}_{\beta}^{d5010} S^{sun} L^{sun} + \mathbf{D}_{\beta}^{i145} S^{sun} L^{sun} \qquad \textbf{(6-32)}$$

The vector $\mathbf{D}_{\beta}^{d5010}$ is column β of the DCM $\mathbf{D}^{d5010}$ for the point on the hemisphere nearest to the actually occurring sun position. The procedure for deriving the illuminances was as follows:

- Load TRY data - then the following operations were carried out for each hour of the TRY where the global irradiance (I_{gh}) was greater than zero.
- Convert irradiances to illuminances using a luminous efficacy model.
- Generate the sun position from the geographical location and time-stamp of the TRY data.
- Generate the sky luminance at the 145 patch centres on the sky vault.
- For the indirect DCM ($\mathbf{D}^{i145}$), locate the patch nearest to the sun position. This is for the indirect component of illuminance from the sun.
- For the direct sun DCM ($\mathbf{D}^{d5010}$), locate the point nearest to the sun position. This is for the direct component of illuminance from the sun.
- Compute the illuminance components using Eq 6-32.

For the Kew TRY, there were 4,406 hours (i.e. unique values) where $I_{gh} > 0$. The internal illuminance at the six photocell locations of the BRE office was derived from daylight coefficients for all these hours. A number of these

illuminances were either too small to be of practical use and/or they occurred outside of normal working hours. The computational overhead of calculating them however was slight. The mean displacement between the 4,406 calculated sun positions and the nearest point on the hemisphere (for the direct sun component) was 0.77˚, with a standard deviation of 0.28˚. The maximum displacement of the sun position was 1.41˚.

The move from a static daylight factor analysis to one based on hourly illuminance values for an entire year necessitates a substantial leap in complexity, for both data analysis/reduction and interpretation. For example, the BRE office has six calculation points (i.e. photocell locations), resulting in a total of 6 x 4,406 ≅ 26,500 derived illuminance predictions. It is a quite straightforward matter to reduce a time-series of illuminance values to a handful of summary metrics. For example, the percentage of the working year for which a target illuminance, say 500 lux, is achieved at each of the calculation points. Summary metrics are useful as ultimate indicators of performance, but significant and/or instructive features of the original dataset may be lost. For the work described here, a gradual 'sifting' of the data is preferable. To this end, a hierarchical approach to data reduction - involving visualisation - was employed. The formats used to present/ analyse the data were:

- MAP is a false-colour map (365 x 24) of the 'raw' hourly values for the year, e.g. illuminances derived from DCs.
- FRQ is a frequency histogram of the incidence (i.e. number of hours) of binned values. It is derived from the 'raw' hourly values, but it can be set to include only those data that fulfil arbitrary criteria. For example, only those illuminances that occur during working hours.
- CML is a curve of the cumulative total - usually calculated using the same criteria as the frequency histogram.

When applied to daylighting quantities, these formats are referred to collectively as 'annual daylighting profiles' (ADPs).

XDAPS

As the suite of programs and scripts that were created for each individual analysis grew, it became desirable to generalise the function of key routines so that they could be re-used for different applications/analyses. From this emerged the "e**X**tensible **DA**ylight **P**rediction **S**ystem" (**XDAPS**). The system is an evolving toolkit of data analysis/visualisation procedures written in the IDL programming language and the UNIX C-shell. The individual programs carry out a range of tasks including:

- Generation of *Radiance* format source descriptions and ray vector co-ordinates for the DC simulations.
- Management of the DC simulations.
- Transformations from Cartesian to spherical co-ordinates (polar and altitude-azimuth).
- Calculation of sun position from time and geographical location.
- Luminous efficacy models.
- Generation and normalisation of sky luminance distributions from sky models and sky model blends.
- Derivation of hourly-annual illuminances from daylight coefficients using Test Reference Year irradiance time-series.
- Analysis and visualisation (with hardcopy) of hourly-annual illuminances, e.g. false-colour maps (365 x 24 arrays) of illuminances, frequency histograms and cumulative values.
- Parametric analyses of hourly-annual illuminances as a function of building orientation.

Most of the above tasks are handled by IDL procedures; UNIX scripts are used to manage the *Radiance* simulations that predict the DC coefficients. The system offers an effective software environment to rapidly prototype analysis scenarios.[17] Using a moderately powered computer (Sparc Ultra 10), XDAPS can derive internal illuminance predictions for the BRE office at

a rate of ~100 skies per second using pre-calculated coefficients. That processing time includes the generation and normalisation of sky luminance distributions from TRY data. It takes therefore ~40 seconds to derive the illuminances for the daylight hours for one year.

6.4.3 Example 1: Introduction to ADPs

The procedure to derive illuminance ADPs for the BRE office is described in this section. For this example, the glazing normal was set to exactly due South. The hourly sky and sun conditions were derived from the irradiance data of the Kew TRY. The diffuse horizontal and direct normal irradiances for this TRY are shown using the MAP format in Figure 6-27. Positive irradiances between > 0 and 500 Wm-2 are shaded blue-through-yellow. Zero values are shaded gray. With this format, one can easily appreciate the significant features of the data for the entire year. Most obvious is the daily and seasonal variation for both irradiances. The hour-by-hour variation in the irradiances is also apparent, particularly so for direct normal irradiance. To give the basic quantities needed for the generation of the sky and sun luminances, the irradiances were converted to illuminances using a constant value for luminous efficacy of 120 lm/W.[18]

The sky and sun conditions were generated from the external illuminances and the (calculated) sun position using the intermediate-overcast sky model blend described in Section 5.4.[19] The sky model mixing function f_{in} for the Kew TRY (Section 5.4.2) is given in Figure 6-28. The majority of the skies, 60%, were given the intermediate sky description (blue ■), 24% were given the CIE overcast sky description (red ■). The remainder, 16%, used an

17. **XDAPS** is used for research and testing within the IESD - it is not intended for general use.

18. Luminous efficacy was not an issue for this work, so a simple model was used. More complex efficacy models could be used, if desired, without adding significantly to the computational effort.

19. For the test described in Chapter 5, the clear-overcast blend performed marginally better than the intermediate-overcast blend. However it was noted that in Section 5.4.3 that the clear-overcast blend may result in composite luminance patterns that are unrealistic. For this reason, the intermediate-overcast blend is used here.

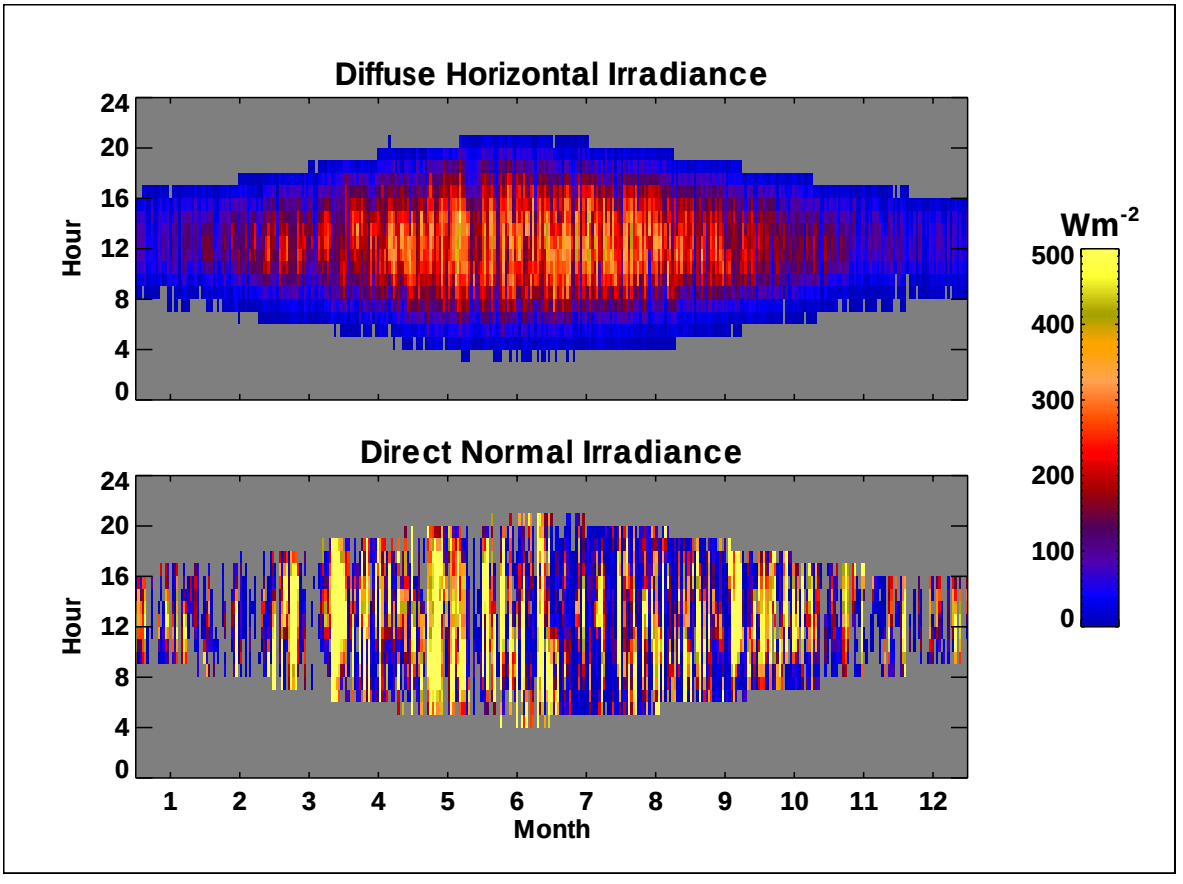

Figure 6-27. Key TRY time series maps

overcast-intermediate blend, the relative proportions for which depended on the sky clearness index (green ■ and transitional shades).

Using the procedure outlined in Section 6.4.2, internal illuminances at the six photocell locations in the BRE office were derived from DCMs. To reduce the number of plots, the ADPs at just one of the photocell locations (p_cell 3) are shown in Figure 6-29. The first of the ADPs, the MAP format at the top of the figure, gives an overview of the hourly illuminance predictions for the whole year. Note that the highest illuminances, ≥2500 lux, occur around noon for the winter months. Next, the FRQ format ADP, shows the number of hours that a (binned) illuminance occurred during the working day, i.e. 09h00 to 18h00. The binsize used for this plot was 50 lux. The last of profiles, CML, shows the cumulative illuminance expressed as a

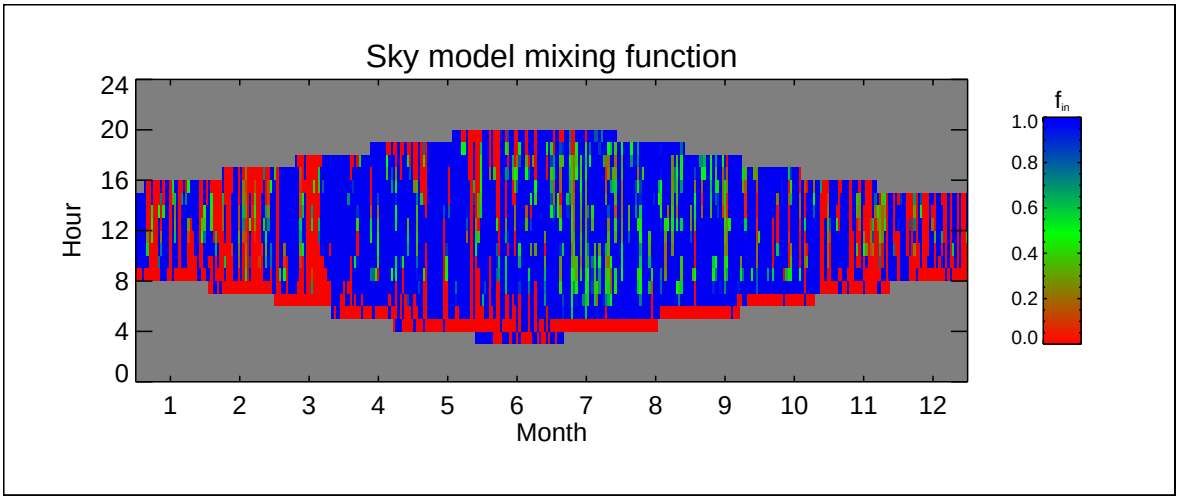

Figure 6-28. Sky model mixing function

percentage of the working year. For example, the illuminance levels: 100, 200, 500 and 1000 lux were attained for (approx.) 90, 80, 65 and 40% of the working year, respectively, at p_cell3.

Recall that the internal illuminance was computed as four distinct illuminance components (Eq 6-32). The MAP format ADPs for the individual illuminance components are shown in Figure 6-30. The high illuminances identified in the MAP for the total illuminance (Figure 6-29) were, of course, due to direct illumination by the sun. For daylighting evaluation, it may well prove useful to analyse both the relative proportions and the magnitude of the illuminance components, e.g. for the ability of a light shelf to redirect sunlight compared to ordinary glazing. The next ADP example shows how a fundamental property of DCs can be exploited to yield an immense quantity of daylighting performance information.

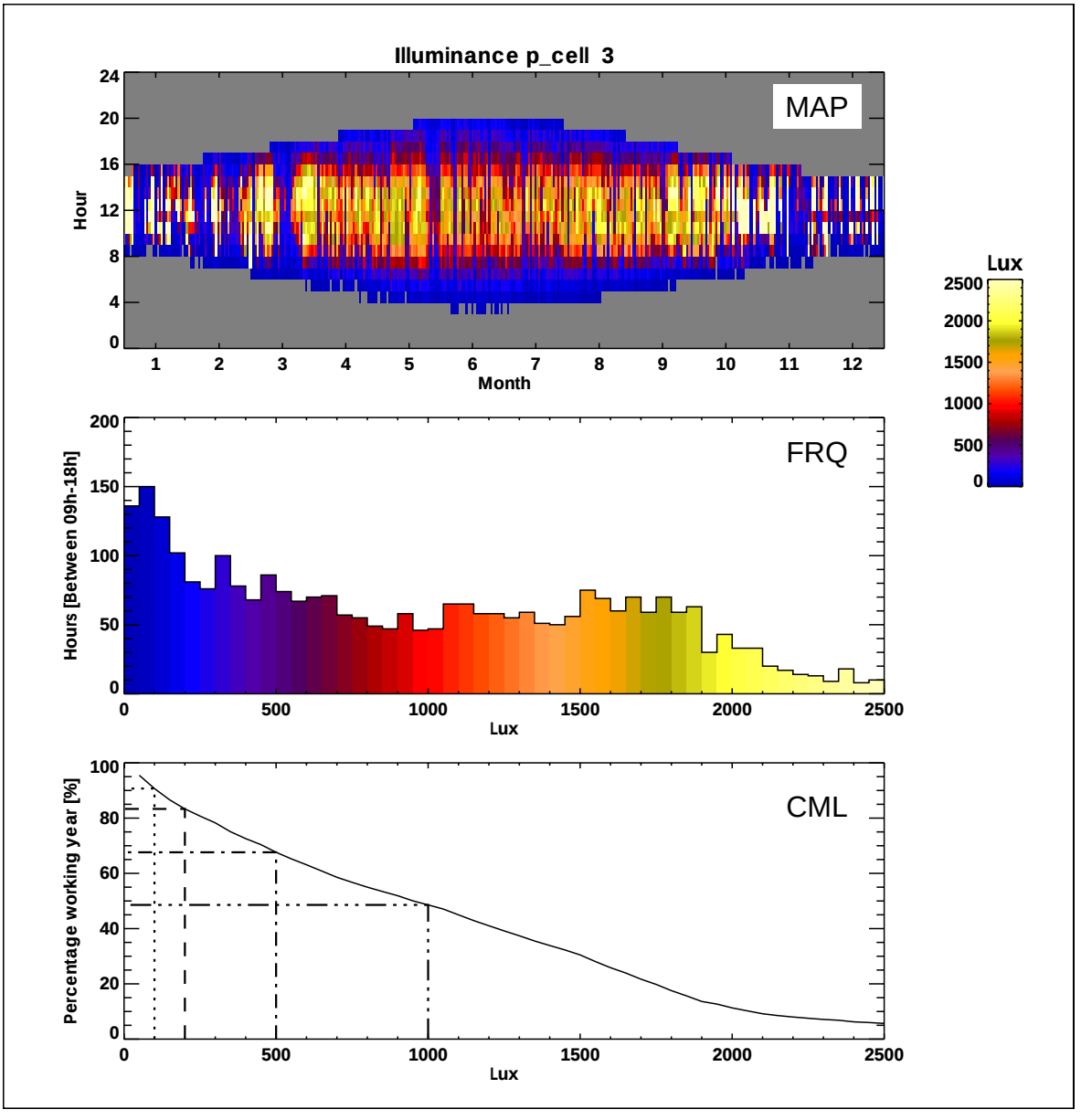

Figure 6-29. DC derived illuminances for p_cell 3 (south glazing)

6.4.4 Example 2: Parametric evaluation of ADPs

For a fixed building configuration, the daylight coefficient matrix is invariant to the building orientation. In other words, once the DCMs have been evaluated, internal illuminances can be derived for arbitrary building orientations by simply applying a rotational transformation to the generated sky-point and sun luminances, Figure 6-31. Consequently, it is a relatively

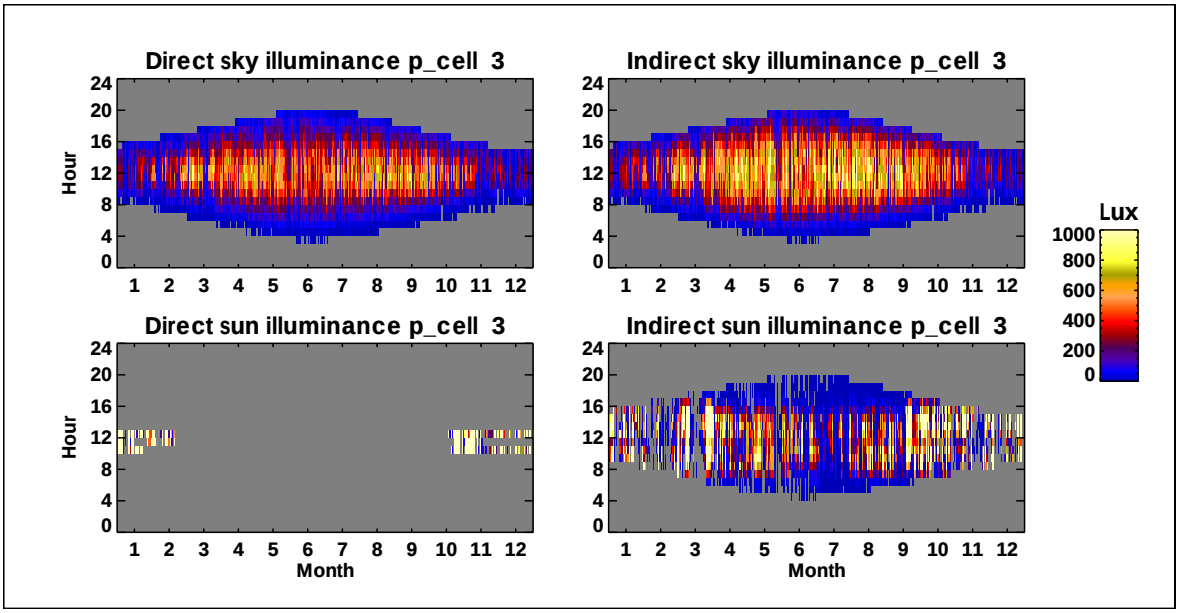

Figure 6-30. DC derived illuminance components

trivial matter to automate the derivation of internal illuminances for a range of arbitrary building orientations. The procedure used for the previous example was modified to predict ADPs for all building orientations in steps of 30˚, i.e. 12 orientations in total. The predictions are presented as a series of 'ADP-roses', one each for the MAP, FRQ and CML formats. In the first instance, predictions for just one calculation point (p_cell3) are shown to limit the number of graphs. The first of these is the MAP-rose, Figure 6-32. The orientation of each MAP in the figure indicates the orientation of the glazing normal for the office model. The sensitivity of daylight illumination to orientation is readily apparent. The anisotropic nature of the sky luminance distributions (and sun conditions) that were used for many of the individual skies is echoed in the patterns of internal illuminance. Note the large difference in overall magnitude for illuminances between the North and South orientations, and the difference in the patterns for illuminance between the East and West orientations. Of course, none of these effects could be reproduced using the standard daylight factor approach. Proceeding as with the first ADP example, the next stage is the 'FRQ-rose',

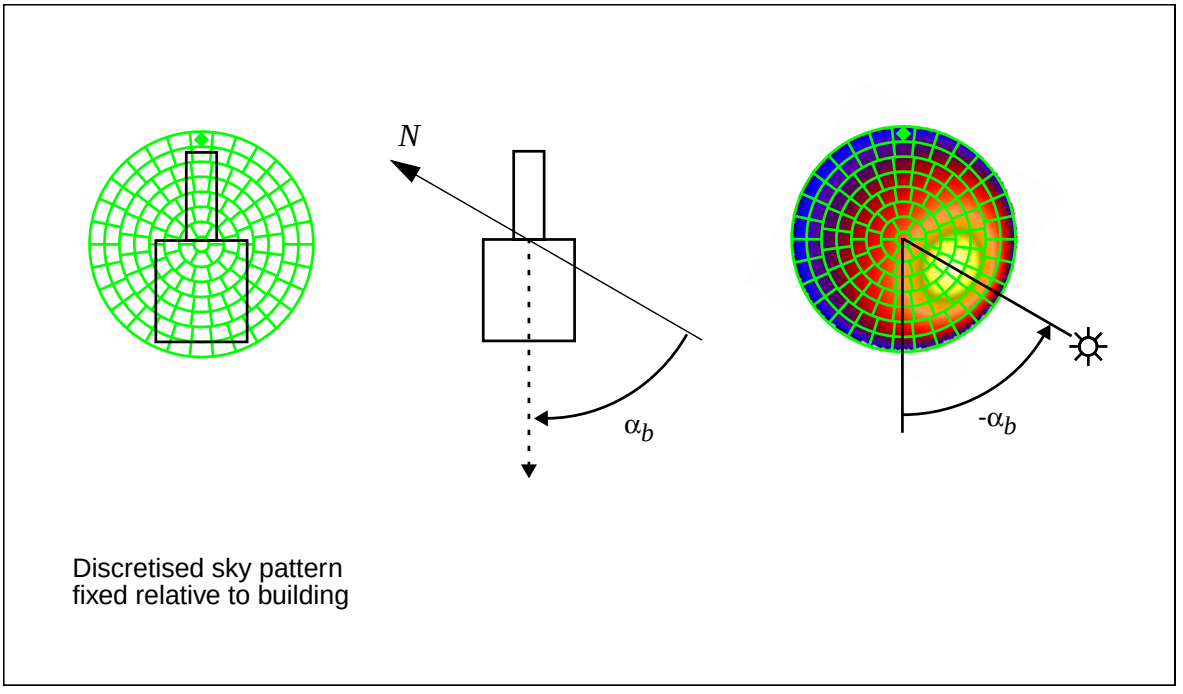

Figure 6-31. Rotation-invariant nature of the DCM

The effect of arbitrary building rotation α_b is achieved by transforming the azimuth of the sun by $-\alpha_b$. Illustration shows building rotated 60˚ West of South and the noonday sun location.

showing the binned occurrence of predicted illuminances as a function of building orientation, Figure 6-33. And then the cumulative totals 'CML-rose' in Figure 6-34. As in Figure 6-29, the cumulative availability of four 'target' illuminances - 100, 200, 500 and 1,000 lux - for each building orientation is marked on the curves.

The cumulative availability of the 'target' illuminances for all six photocells as a function of building orientation is shown in a highly compact form in Figure 6-35. This type of plot is referred to here as the 'target' illuminance or TI-rose. For this example, a total of 317,232 (= 4406 x 12 x 6) illuminance predictions were derived from just the one set of DCMs. In fact, because the four illuminance components were computed separately, the total number of internal illuminance predictions was ~1.2 million.

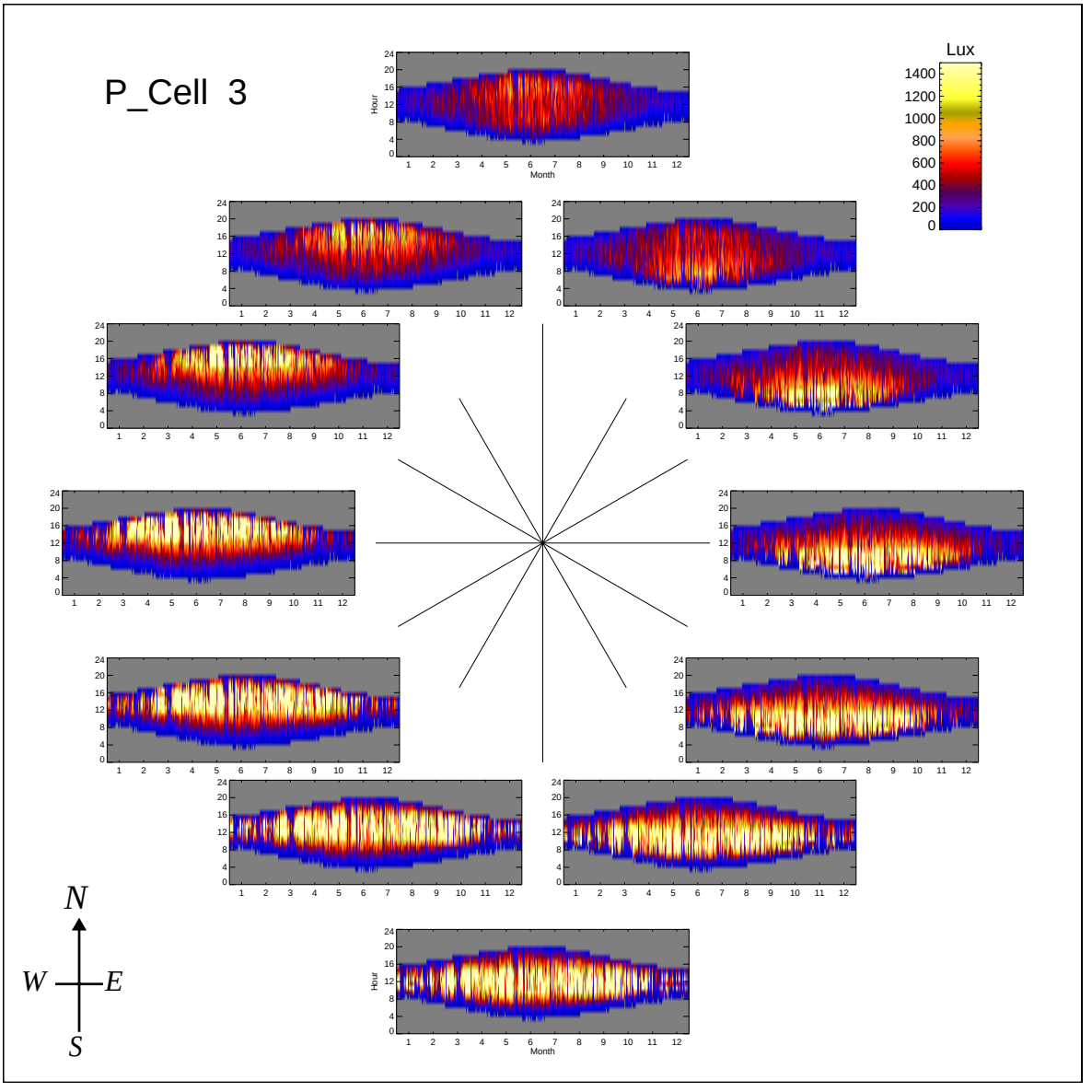

Figure 6-32. 'MAP-rose' for p_cell3

6.4.5 Example 3: ADPs and the daylight factor method

Daylight coefficient derived cumulative illuminances for one year could be compared with cumulative estimates based on daylight factor values (Section 6.1.1). Provided of course that the same TRY was used for both analyses. A straightforward comparison between a DC derived cumulative illuminance and one based on daylight factors is problematic because they are not identical quantities. The daylight factor approach to annual

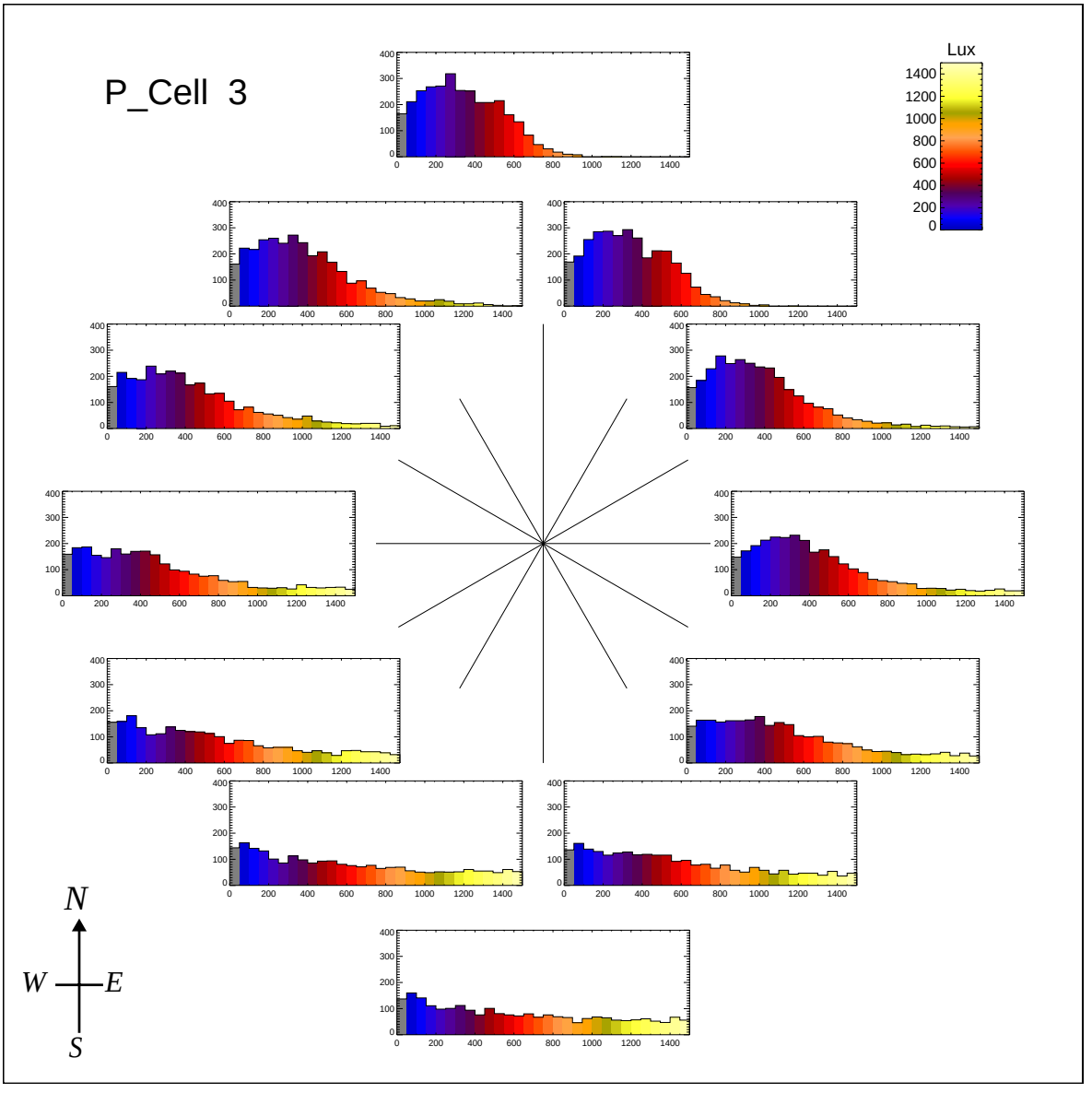

Figure 6-33. 'FRQ-rose' for p_cell3

estimates considers only the *diffuse* illuminance availability (Figure 6-2). One could argue therefore that results from this simple approach should only be compared with the DC derived illuminance for the sky component, i.e. just two of the four components shown in Figure 6-30. Whilst this might be considered as comparing like-with-like, the sky only illuminance is in reality a somewhat abstract quantity of qualified physical significance. This is so because, for real buildings, it is almost impossible to exclude the

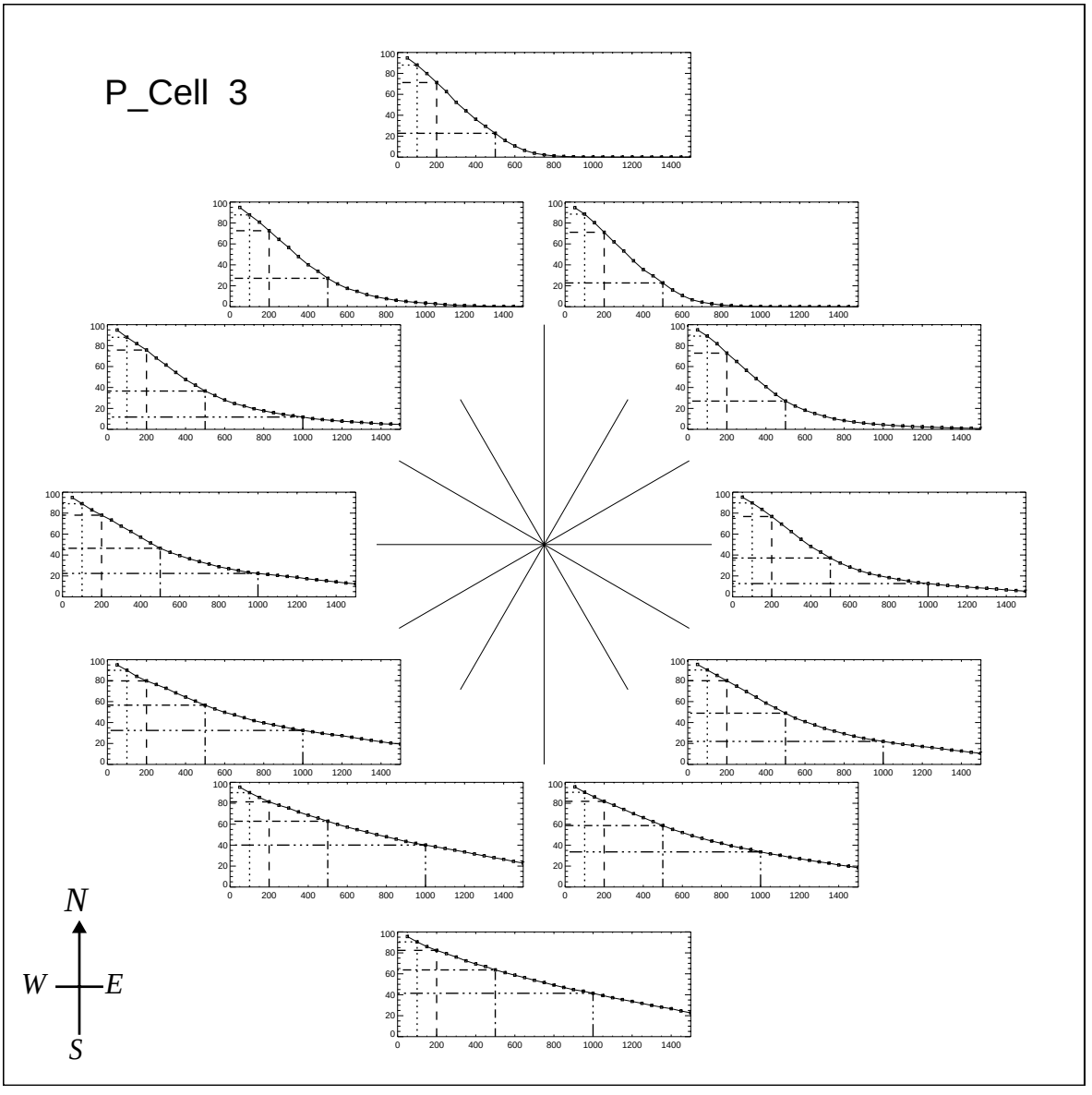

Figure 6-34. 'CML-rose' for p_cell3

illumination effects of sunlight - particularly indirect - for a fixed building/ glazing design. Indeed, from the MAPs shown in Figure 6-30 it is clear that, for this orientation at least, the indirect sun illuminance was a significant (if erratic) contributor to the total annual illuminance.

As noted previously, the ratio of internal to external illuminance varies greatly under real skies [Tregenza 83]. This ratio is called here the 'Total Daylight Factor' (TDF) because it is based on the total internal illuminance,

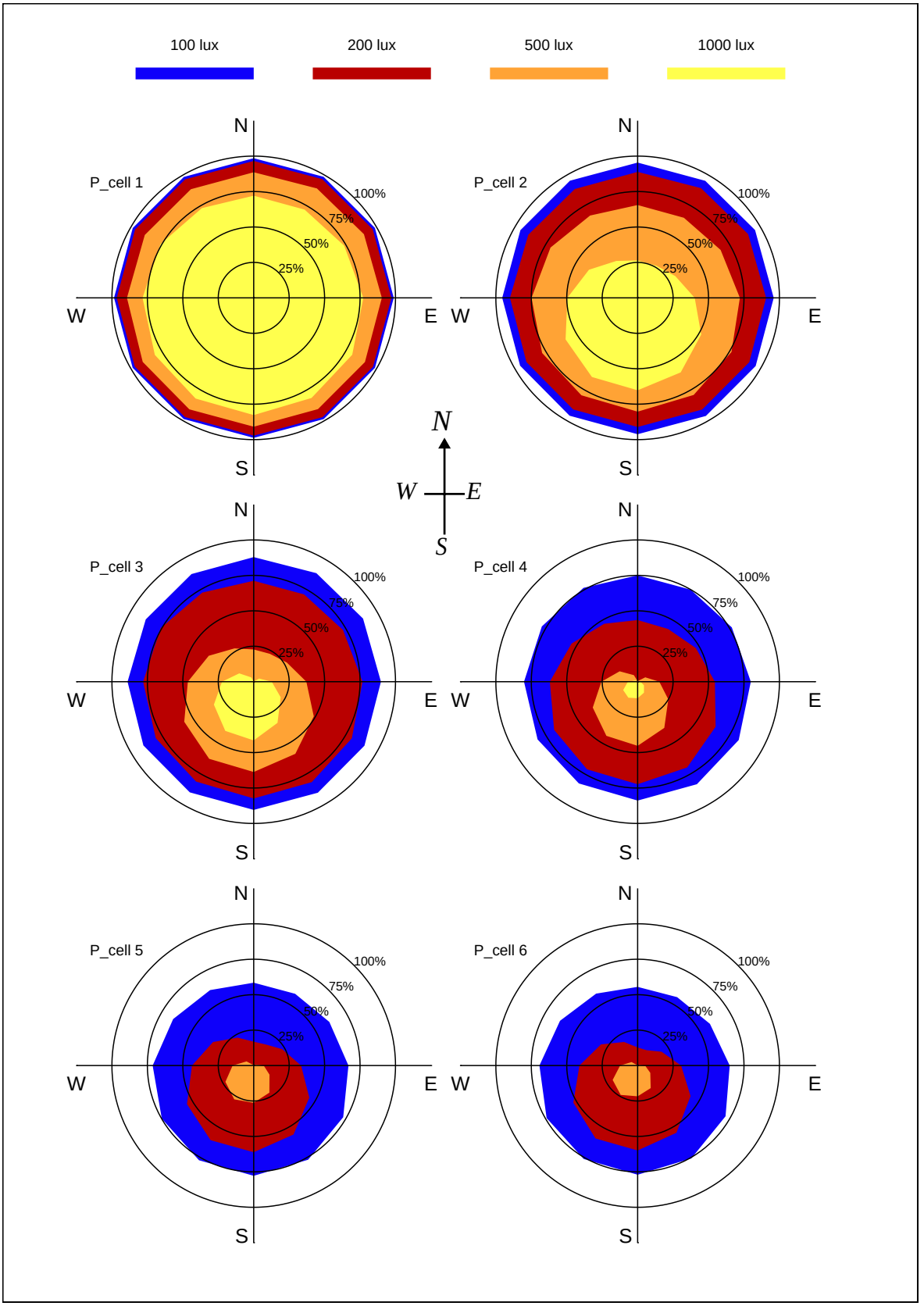

Figure 6-35. 'TI-rose' for all photocells

i.e. direct and indirect for both sky and sun. The hourly TDFs at p_cell 2 in the BRE office were derived from the illuminance predictions shown in Figure 6-32 and the Kew TRY. The distribution in TDFs as a function of glazing orientation is shown in Figure 6-36. This distribution provides a

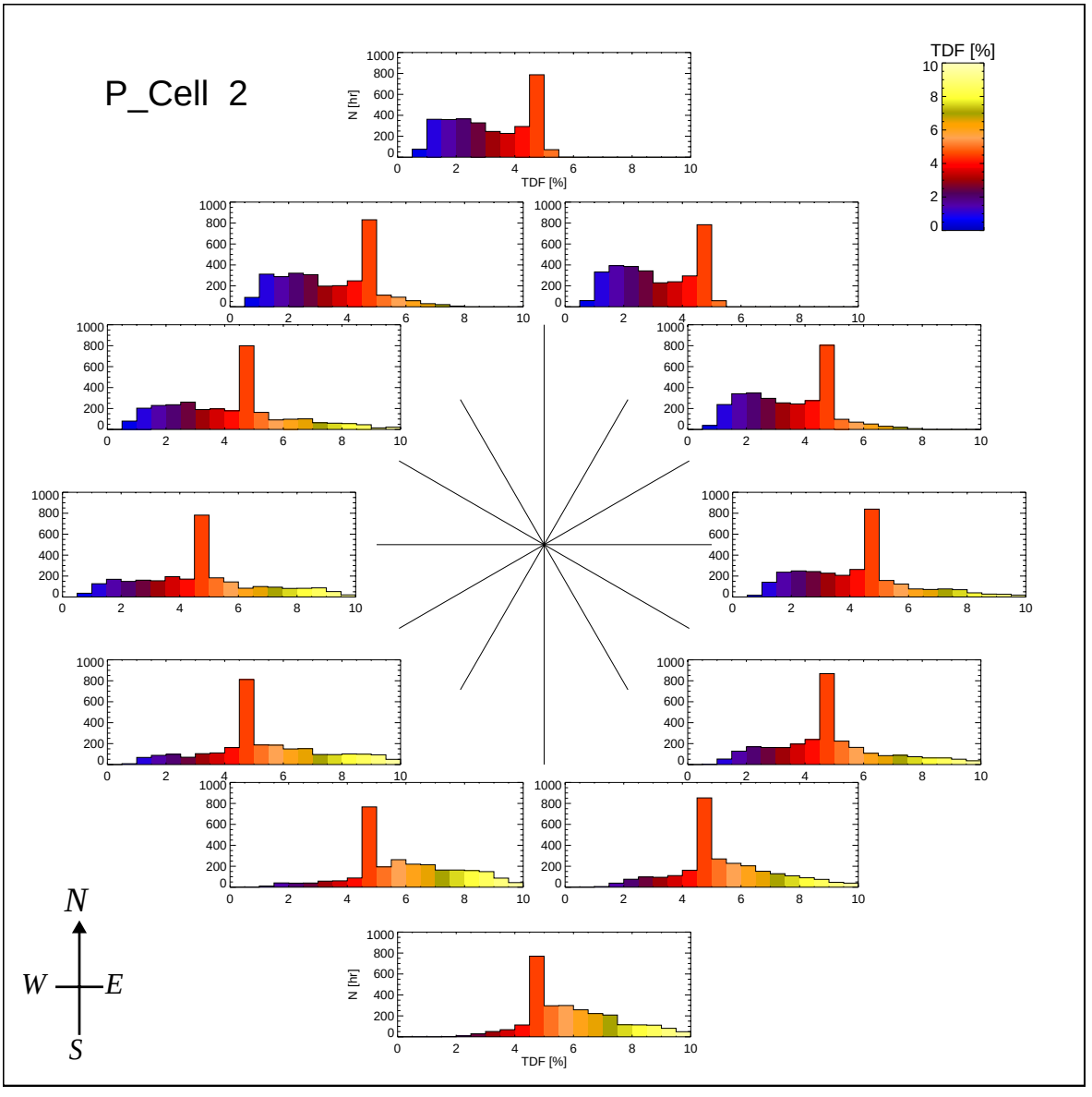

Figure 6-36. Frequency distribution of predicted TDFs as a function of glazing orientation

measure of the deviation between the TDFs and the standard daylight factor (SDF) based on the CIE Standard Overcast Sky. The most prominent feature of the distributions is the peak centred on TDF = 4.75%. The peak is of

similar size - approx. 800 hours (i.e. skies) - for all the glazing orientations. For the TDFs that were counted in this bin, the corresponding illuminances were derived from DCs using the overcast sky description. This TDF therefore is the standard daylight factor (SDF) as it would be calculated using traditional techniques.

The deviation between the TDFs and the SDF is examined in more detail in Figure 6-37. Three glazing orientations from Figure 6-36 are used for illustration - North, East and South. The luminance distributions for an overcast and an intermediate sky are included as shaded surfaces at the bottom of the figure. These two skies were normalised to give the same diffuse horizontal illuminance, and they are shown using identical scaling. The difference in the distribution of TDFs as a function of glazing orientation is explained as follows. Consider first those irradiance values in the Kew TRY that resulted in overcast sky conditions with no significant sun component (using the sky blending rule described in Section 5.4.2). For these instances in the TRY, the sky luminance distribution used to derive internal illuminances was that of the CIE standard overcast sky. Thus, for these skies, the ratio of internal illuminance to external illuminance was a constant: identical to the standard daylight factor. The CIE overcast sky is, of course, symmetric about the z-axis, so these TDFs were the same for all orientations. Next, consider those instances where the sky conditions were determined to be largely non-overcast (i.e. intermediate). For these, the maximum sky luminance was concentrated about the sun position, which for the most part was in the South. Also, there was the contribution of - mainly indirect - sunlight. The luminance of the sky in the North is, for the non-overcast (i.e. intermediate) model, lower than that for an equivalent (i.e. same diffuse horizontal illuminance) overcast sky (around midday), see Figure 6-37. Relative to the SDF therefore, TDFs for non-overcast (i.e. intermediate) skies were lower for a North glazing orientation and higher for the South glazing orientation. For the East (and West) glazing orientations, the distribution was a mixture of those for the North and South. The East

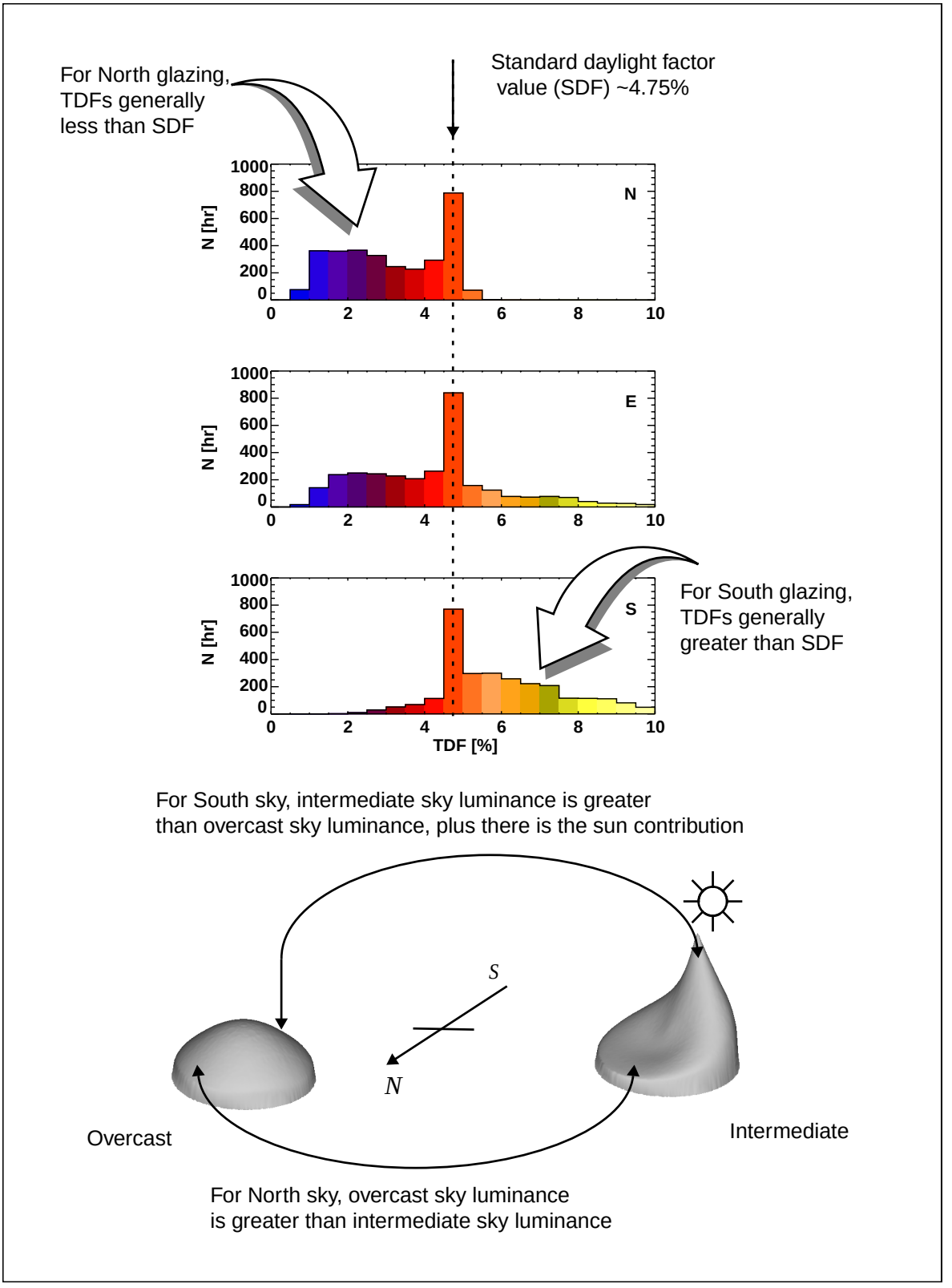

Figure 6-37. Examination of TDF distributions for three orientations

Example overcast and intermediate skies produce the same (diffuse) horizontal illuminance

orientation was just as likely to have the sun with a bright circumsolar region 'in front of' the glazing in the morning as it was to have the lower luminance sky, opposite the sun, 'in front of' the glazing in the evening.

The numbers in the TDF distribution will be sensitive to the sky model(s) used, but the general observations are likely to remain the same. This is because they are a consequence of the fundamental difference between the Standard Overcast Sky (peak luminance at the zenith) and the non-overcast models (peak luminance at the sun position). Furthermore, since evidence has been presented to the effect that the overcast-intermediate blend offers a plausible representation of naturally occurring sky conditions (Section 5.4), a reasonable conclusion from this exercise is that actually occurring TDFs are likely to vary significantly from the (static) SDF value - as shown in Figure 6-36. This observation in itself is nothing new [Tregenza 83]. The significance of the analysis presented here is that it is now possible to quantify the discrepancy to a high degree of precision - controversy regarding sky models notwithstanding. The analysis does not have to make use of sky models, the luminance distribution could equally be based on actual measurements, as it was for the validation. Accordingly, it was not the intention here to suggest that the overcast-intermediate sky model that was used to derive the TDFs is the 'best' sky model combination to use for the Kew TRY, or any other Test Reference Year. Rather, this example has demonstrated one aspect of a new schema for the investigation and, importantly, validation of daylight prediction techniques.

6.4.6 Implementation and application issues

In this section, issues relating to the practical and research use of the daylight coefficient approach are discussed.

Variable Building or Glazing Configurations

Any change to a building that alters the passage of daylight into a space creates, in effect, a new building configuration. Ideally, each unique

building configuration would require its own unique set of DCMs. Changes to the building configuration can be effected by any of the following:

- user-operated venetian blinds;
- a motorised shading screen that automatically responds to illumination levels; and,
- responsive glazing systems e.g. photochromic (passive) or electrochromic (active).[20]

For a continuously variable property, such as the angle and/or extent of a motorised shading screen, the full range of variation would have to be modelled as a limited number of incremental changes in building configuration. If the number of discrete configurations is large, then the potential advantage of DCs over the standard calculation may be diminished or even eliminated.

Sub-hourly Predictions and Lighting Controls

With a daylight coefficient approach, the prediction of internal illuminances at a sub-hourly timestep is a tractable problem. The issues to consider are the nature of the variability in the meteorological conditions and how they relate to internal illuminance. If the intention is to account for the internal illuminance resulting from small changes in the sun position, then the timestep for the analysis needs to be commensurate with that aim. For example, at the hourly timestep of typical TRYs, the sun moves 15˚ every timestep. Modelling this with a hi-res direct DCM for 5010 points on the hemisphere gives a mean sun displacement angle for the year of less than 1˚, which is more than adequate.[21] At a timestep of 5 minutes, the sun moves approximately 1.2˚ every timestep, which is close to the typical sun

20. If it is only the glazing transmissivity that changes, and the change is applied equally to all the glazing elements, then it may be possible to model this scenario with just one set of DCMs by adjusting the internal illuminance levels in response to the glazing transmissivity.

21. The typical sun displacement angle is about half the angular spacing of the points across the hemisphere. For 5000 points the angular spacing is about 2˚.

displacement angle for the 5010 point DCM. Is there any advantage in modelling the sun position to a higher degree of accuracy, regardless of the timestep used? The answer is - almost certainly no. There is little practical value in resolving internal illuminance levels at very fine *spatial* scales. However, there is value in obtaining illuminance levels at very fine *temporal* scales. Here it is the short-term variability of internal illuminance levels in response to rapidly changing sky and sun brightness conditions that is the issue, rather than variability which is due solely to the changing sun position.

Everyday experience informs us that sky and sun brightness conditions change at timescales much shorter than the hourly timestep of TRYs. Whilst the evaluation of daylight illumination based on ADPs offers a significant advance over the standard daylight factor approach, the modelling of daylight responsive systems needs to be carried out at *the timescale at which the systems are likely to respond*. This is particularly important for the modelling of lighting control systems which are intended to respond to changes in daylight illumination levels. With a DC based approach, the prediction of daylight illuminance levels at a timestep as short as even 1 minute, for long time periods, is a practical possibility. Thus, the long-term behaviour of arbitrary lighting control algorithms can be predicted.

Luminous Efficacy and Sky Model Performance

The sky luminance distributions used in the derivation of ADPs will generally be based on basic irradiance quantities, such as the Kew TRY (examples Section 6.4.3 to Section 6.4.5). Thus, the ADPs that are derived will be sensitive to the luminous efficacy models and the sky models that are used. Luminous efficacy is known to vary depending on several factors including sky conditions (e.g. clear, overcast) and source type (i.e. direct sun or diffuse sky) [Littlefair 88].

For sky models, there are several types that are currently in use. Testing of these models has only recently taken place with the availability of measured

sky luminance distributions [Ineichen 94][Littlefair 94]. The validation has generally been based on the ability of the models to reproduce measured sky luminances. Another approach to validation is to examine the effect of sky model type on *internal illuminance*. Based on the work described in this thesis, it is now possible to accurately - and efficiently - predict the sensitivity of internal illuminance to both luminous efficacy and sky model type. Making full use of each set of DCMs, it is possible to efficiently investigate the effects of building orientation and different climatic zones over an analysis period of a full year at an hour (or better) timestep. The potential to generate such a wealth of reliable internal illuminance data from a relatively small number of lighting simulations is unprecedented.

Design Guides

The rotation-invariant nature of DCMs means that, once the DCM has been computed, the sensitivity of daylight illumination to building orientation can be determined at minimal expense (Section 6.4.4). Furthermore, illuminances can be derived from DCMs using arbitrary Test Reference Years for any geographical locale. For example, it would be a relatively trivial matter to reproduce the TI-rose analysis (Figure 6-35) for a wide range of prevailing climatic conditions covering Europe, or even further afield. The daylight part of design guides - such as the LT method [Baker 94] - could be significantly improved if these techniques were to replace the daylight factor based methods used for the original analyses.

DC derived ADPs: End-User Software

The following questions concerning implementation of the DC approach need to addressed if it is to gain wider acceptance. Firstly, is it practicable to embed the daylight coefficient scheme in end-user software? Secondly, to what degree can the intricacies of the technique be hidden from a prospective (i.e. non-expert) user?

If it is practicable for a non-expert user to calculate daylight factors accurately using *Radiance*, then daylight coefficients should not prove to be

too difficult. The main problem - for either daylight factor or daylight coefficient calculation - is the setting of the ambient parameters (Section 3.3.2). If this can be achieved reliably, then automation of the prediction of DCMs is a relatively straightforward matter which can be largely hidden from the user. It is possible to provide some general guidance for the setting of the ambient parameters. However, optimum values for the parameters are largely scene dependant, so some insight and/or experimentation is usually needed to achieve the best effect.

These issues notwithstanding, the IESD have produced a *Radiance*-based software tool to predict time varying illuminances called the Dynamic Lighting System [EPSRC 97]. The work described in this chapter formed the basis of the 'calculation engine' for the Dynamic Lighting System (DLS). At the time of writing, the DLS was about to be released for beta-testing. It is hoped that the daylight coefficient approach described here will be incorporated into other *Radiance*-based software packages.

DC derived ADPs: A Benchmark for Evaluating Simpler Methods

Sufficient evidence has been presented in this chapter to demonstrate that daylight coefficient based analyses offer a major advance over established techniques. The uncertainties, such as they are, are those relating to luminous efficacy and sky models, and not with the DC approach itself. It seems reasonable therefore to propose that DC based ADPs become the benchmark against which predictions for long-term daylighting performance using simpler techniques are compared. Making comparisons however, is unlikely to be straightforward. Largely because it is dissimilar quantities that will be under consideration (see Section 6.4.5). It likely that a new set of daylighting metrics will need to be formulated before these issues can be resolved. What form these metrics may take is discussed below.

Refinement of ADPs

The ADPs that have been described thus far need to be refined before they can be of practical use to lighting designers. The fundamental inadequacy of the ADPs, as described above, is that each point of calculation is treated *independently*. What is needed is a class of measures, based on the hourly illuminance predictions, that account for the entirety of the space. For example, a quantity of key importance for daylighting is the uniformity of illumination across the work plane. It would be a trivial matter to calculate, for each hour, the uniformity ratio for a space based on the hourly illuminance predictions at each calculation point. The uniformity ratio on its own however is less than ideal because it does not give any indication of *useful* levels of illumination. A more helpful measure would make account of both uniformity *and* absolute illuminance levels. A term for these hypothesised measures is offered: 'Total Daylighting Performance Metrics' (TDPMs). Note that TDPMs could be formulated to account for both absolute *and* relative levels of any (or all) of the four illuminance components.[22] By treating the sun illuminance components separately, the performance of an innovative glazing system could be assessed in terms of both shading *and* re-direction of solar beam radiation.

To be truly comprehensive, TDPMs would need to make account of field-of-view luminances also. This could be the luminance for points across the principal wall surfaces, and perhaps across the glazing also. Luminance TDPMs would be calculated for the same period and timestep as the illuminances. How luminance TDPMs might be formulated is described in a paper presented by the author at the 1998 National Lighting Conference [Mardaljevic 98]. Aside from a few suggestions as to what quantities TDPMs might make account of, the formulation of TDPMs is likely to be a significant task and beyond the scope of this thesis.

22. If they are based on illuminances derived using the *Radiance* DC formulation.

6.5 Conclusion

The accurate and efficient prediction of hourly internal illuminances for a full year is now a practical possibility using daylight coefficients. This chapter has demonstrated how the *Radiance* lighting simulation system can be used to predict the daylight coefficients from which internal daylight illuminances are derived. Several variants of the daylight coefficient implementation were investigated. The magnitude and form of the daylight coefficient matrices were related to the building configuration and the discretisation scheme. The accuracy of the derived illuminance predictions was verified using the BRE-IDMP validation dataset. The daylight coefficient implementation was then generalised so that hourly daylight illuminances could be predicted from Test Reference Year time-series data. Hourly illuminance predictions for a full year were presented using three different formats demonstrating a progressive reduction of the data. The rotation invariant nature of the DCM was made use of in an example that predicted the annual daylighting profile as a function of building orientation. A range of implementation and application issues were discussed.